Supplementary Material to paper 'Reservoir storage and hydrologic responses to droughts in the Paraná River Basin, Southeast Brazil'

Davi C. D. Melo[1,2], **Bridget R. Scanlon**[2], **Zizhan Zhang**[2], **and Edson Wendland**[1]

[1]Department of Hydraulic and Sanitary Engineering, University of São Paulo, Avenida Trabalhador São-carlense, 400 - Parque Arnold Schimidt, São Carlos - SP, 13566-590, Brazil
[2]Bureau of Economic Geology, University of Texas at Austin, 10100 Burnet Rd, Austin, TX 78758, USA

Correspondence to: Davi Melo (melo.dcd@gmail.com)

Contents

List of Figures

List of Tables

S1 Introduction

This document consists of four sections containing supplementary information and materials about the study area (Section S2); ground-based and remotely sensed data (Section S3); methods used for data processing (Section S4); and results (Section S5).

S2 Study area

S2.1 Droughts in southeastern Brazil

Drought events in the Paraná Basin (PB) have great impacts not only on human water supply but can also compromise crop production and hydropower generation (Helmer and Hilhorst, 2006; Lima and Lall, 2010). About 65 % people in Brazil reside in the PB, with a total water demand of $\sim 23\,\mathrm{km^3\,yr^{-1}}$ (ANA, 2010). According to São Paulo's Agricultural Institute (http://www.iea.sp.gov.br), the agricultural losses due to the 2014 drought were the worst in the past 50 years. Hydroelectric plants supply ~ 65 % of Brazilian demand for electricity (ANA, 2010). The hydroelectric plants in the state of São Paulo's alone account for ~ 18 % of Brazil's installed capacity. The 13 largest dams in the Paraná basin (PB) generate ~ 160 TWh per year (Section S2.2), including Itaipu responsible for ~ 35 % of the generation.

Some recent articles addressed this issue in the region. Coelho et al. (2015a) analyzed ~ 55 years of rainfall records over the region of Sã Paulo city. Their findings show previous dry events since the 1960s but none exceeds the magnitude of the 2014 drought in terms of precipitation deficits, making the 2014 drought the driest event since 1962.

According to Coelho et al. (2015b), the 2014 drought originated from anomalous rainfall in Northern Australia, which resulted in a sequence of events that connected the tropical and extratropical regions of the Pacific Ocean until it reached southeast Brazil. These events caused an anomalous high pressure system over the Atlantic, forcing an oceanic trajectory of the frontal systems and the humidity from Amazon to migrate to Southern Brazil, which prevented the formation of precipitation events in the South Atlantic Convergence Zone (Coelho et al., 2015b). Coutinho et al. (2015) analyzed the regime shifts in the reservoirs of the Cantareira system caused by droughts. Based on the relation between rainfall and water storage in the reservoirs, they built a mathematical model and showed that the mechanism that controls the reservoir dynamics has changed. Getirana (2015) used remotely sensed TWS anomaly (TWSA) data from GRACE to detect and quantify the impacts of the 2014 drought over southeastern and northeastern Brazil. According to his analysis, between 2011 and 2015, a depletion in water storage of $6.1\,\mathrm{cm\,yr^{-1}}$ ($56.4\,\mathrm{km^3\,yr^{-1}}$) occurred over the Southeastern Brazil as a result of lower-than-usual rainfall rates.

S2.2 Hydroelectric generation

Hydroelectric plants (HEP) produce ~ 65 % of all electricity in Brazil, being the Southeast/Middle-West region (SE/MW) the one with the higher generation rates. Most of these plants are inside Paraná basin, including the bi-national Itaipu dam (Brazil-Paraguay), which is one of the largest producer of electricity worldwide (~ 2.3 billion MWh since 1984) (https://www.itaipu.gov.br/energia/geracao). Reports by the Brazilian Electric System National Operator (ONS - Operador Nacional do Sistem Elétrico) show that twelve plants among the 37 analyzed in this study generate ~ 160 TWh $\mathrm{yr^{-1}}$. In 2012, these plants generated 200 TWh (Fig. S1) but since 2013 the production has decreased, although the demand in the SE/MW region continued to increase (Fig. S1).

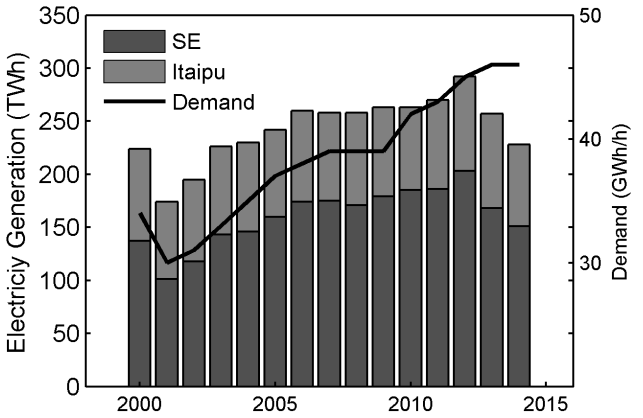

Figure S1. Electric generation and demand in the Southeast (SE) region

Table S1. Historical and projections of population and surface water demand for human supply in the Paraná basin

Year	Population ($\times 1000$)	Demand ($\mathrm{km^3\,yr^{-1}}$)
2005	53,575	2.85
2010	62,120	3.4
2025	68,118	3.8

S2.3 Water demand

The Paraná basin hydrographic region (PB) has ~ 30 % of Brazilian population. Historic data published by Brazilian Water Agency (ANA - Agência Nacional de Águas) shows that the water demand for human supply in 2005 was $2.85\,\mathrm{km^3\,yr^{-1}}$ and is expected to reach $3.8\,\mathrm{km^3\,yr^{-1}}$ in 2025 (Table S1). As shown in Fig. 1 of the manuscript, the PB encompasses areas of seven Brazilian states, two of which (Sã Paulo and Minas Gerais) account for ~ 90 % ($835,000\,\mathrm{km^2}$) of the SE region and have ~ 77 % (65 million people) of the region's population. The water supply in the SE region is composed 47 % of surficial water bodies, 39 % from groundwater and 14 % from mixed (groundwater + surface water) sources (ANA, 2006). The total irrigated area inside PB is $\sim 530,000$ ha, corresponding to ~ 45 % of all irrigation in Brazil. The irrigated area inside PB accounts for ~ 1 % of the basin.

The Paraná hydrographic region is composed by the following sub-basins: Paranaíba, Paraná, Tietê, Paranapanema, Iguaçu and Rio Grande basin (Fig S2). According to the

Brazilian National Water Agency (ANA - Agência Nacional de Águas) the total surface water delivery ($\sum Q_{del}$) is $15\,km^3\,yr^{-1}$ (ANA, 2006). The demand in the Tietê sub-basin corresponded to $\sim 50\,\%$, most of which is for urban and industrial uses ($\sim 40\,\%$ of $\sum Q_{del}$) (Fig S2a). In Brazil, surface water availability is often assessed by means of Q_{95} discharge, that is, the discharge equaled or exceeded for 95 % of the time. The ratio between delivered discharge (Q_{del}) and Q_{95} indicates how stressed the surface water resources are. The most critical situation occurs in the Tietê sub-basin, where $Q_{del}/Q_{95} \sim 65\,\%$ (Figs. S2b, 2c). This sub-basin has the lower surface water availability inside the Paraná basin: 8 % of PB-Q_{95} (Fig. S2c). Most of PB-Q_{95} is found in the Rio Grande and Paraná sub-basins (20 and 29 %, respectively) (ANA, 2006).

Recent data indicate the total water demand in 2010 increased to $23\,km^3\,yr^{-1}$ ($\sim 19\,maf\,yr^{-1}$), which correspond to $\sim 13\,\%$ of PB-Q_{95} (www2.ana.gov.br/Paginas/portais/bacias/parana).

S2.4 Topography, climate and land use

Additional maps of the study area are provided in Fig. S3 to complement those shown in the manuscript. The topography in the Paraná basin (PB) consists, basically, of high plains with maximum altitudes higher than 2,000 m above sea level. Most of PB is under temperate highland tropical climate with dry winters (Cwb) and humid subtropical climate with hot summer (Cfa) or with dry winter (Cwa). Most of the reservoirs are located near the center of the basin, where the land use consists, basically, of annual crops and sugar cane.

S3 Data

S3.1 Reservoirs

Daily data of inflow, water level and storage of 50 reservoirs were downloaded from the Brazilian National Water Agency (ANA - Agência Nacional de Águas) web site for the period Jan 1995 - Jun 2015. The data can be accessed from http://sar.ana.gov.br/MedicaoSIN (last access in 10 Dec 2015).

The 37 reservoirs analyzed in this study are listed in Table S2, along with their geographical coordinates, Brazilian state where they are located, surface area and storage capacity (volume). Daily data of inflow, water level and storage of 50 reservoirs were downloaded from the Brazilian Water Agency (ANA - Agência Nacional de Águas) web site for the period Jan 1995 - Jun 2015. The data can be accessed from http://sar.ana.gov.br/MedicaoSIN (last access in 10 Dec 2015). After a screening process, only 37 reservoirs were considered for analysis. Among the remaining reservoirs, only eight had gaps in the time series: Billings (30 %), Funil (18 %), Jaguari (18 %), Paraibuna (18 %), Tres Marias (17 %), Miranda (15 %), Cachoeira Dourada (9 %) and Corumba I (9 %).

S3.2 Global Land and Data Assimilation System - GLDAS

The Global Land Data Assimilation System is a global, high resolution modelling system (of the Earth land surface) that combines satellite and ground-based observations to constrain the modelled land surface by Land Surface Models (LSM) (Rodell et al., 2004). The LSMs used by GLDAS include the Common Land Model (CLM) (Dai et al., 2003), NOAH (Chen et al., 1996; Ek et al., 2003); the Variable Infiltration Capacity (VIC) model (Liang et al., 1994) and MOSAIC (Koster and Suarez, 1996). GLDAS outputs and forcing data are available in GRIB and NETCDF formats from http://mirador.gsfc.nasa.gov/.

GLDAS uses four land surface and several atmospheric forcing datasets to produce the outputs from these LSMs at 1° and 0.25° (for NOAH) horizontal resolutions and 3-hourly or monthly time resolutions for the period from 1979 to present (GLDAS 1.0) and from 1948 to 2010 (GLDAS 2.0). The land surface datasets consist of high resolution vegetation classification maps (1 km), soils database (5'), elevation database (30') and Leaf Area Index map (1 km) (Rodell et al., 2004). Some examples of atmospheric forcing datasets used by GLDAS are the National Centers for Environmental Prediction's (NCEP) Global Data Assimilation System (GDAS) meteorological data (Derber et al., 1991) and National Aeronautics and Space Administration's (NASA) Goddard Space Flight Center (GSFC) Tropical Rainfall Measuring Mission (TRMM) 3B42V6 rainfall data product (Huffman et al., 2007).

The data is available for both the first version (GLDAS 1.0) and that released in 2013 (GLDAS 2.0). The main difference between these versions is the forcing datasets. In the first version, the forcing data is a (non-overlapping) combination multiple data sets whereas GLDAS 2.0 uses the Global Meteorological Forcing Dataset from Princeton University (Sheffield et al., 2006). A newer version (GLDAS 2.1) is expected to be released in a near future. Given the time period considered in this study, only the data from GLDAS 1.0 were used. The outputs from NOAH were averaged to a 1° grid to match the grid of the other LSMs. Runoff and soil moisture time series simulated by all four LSMs were extracted and averaged over the contributing basin of each reservoir, excluding the contributing area of up-stream reservoirs, when present.

S3.3 Remote sensing products and ground-based precipitation

TRMM data is derived from the measurements of a Precipitation Radar (PR), Microwave imager (TMI) and Visible Infrared Scanner aboard on the satellite. TMPA rain-

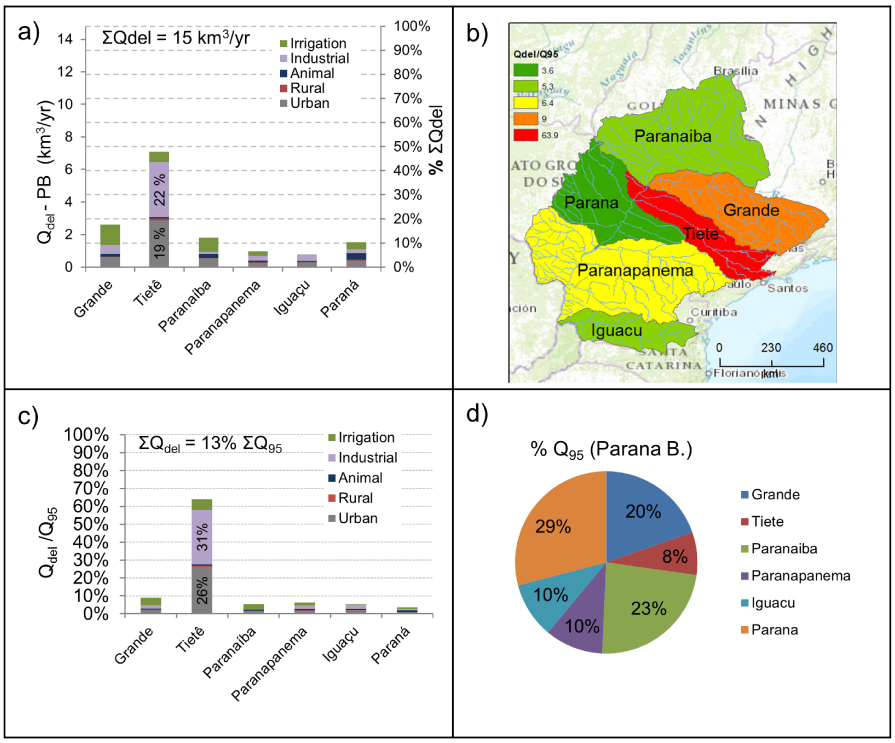

Figure S2. Surface water deliveries (Q_{del}) for different uses per sub-basin (a); Q_{del}/Q_{95} per sub-basin (b); distribution ofQ_{del}/Q_{95} for different uses; contribution of each sub-basin to Q_{95} in the Paraná Hydrographic region

fall estimates are based on the combination of TRMM data with high quality passive-microwave-based rain estimates from orbiting satellites calibrated by TRMM's PR and TMI (NASA, 2011). To fill in eventual remaining gaps, IR data from five geosynchronous satellites covering the tropics are used. TMPA monthly estimates were chosen to complete the rainfall time series because they showed satisfactory performance (index of agreement ~ 0.75) compared to ground-based gridded data in the study area (Melo et al., 2015).

Remotely sensed rainfall estimates (P_{Sat}) were derived from TRMM Multisatellite Precipitation Analysis (TMPA) 3B43 version 7 product, which merges 3B42 estimates and gauge-data into a single rain product (Huffman et al., 2007). Past studies have shown satisfactory performance of TMPA rainfall estimates and, thus, it was chosen to complete the rainfall series for the study period. Melo et al. (2015) compared monthly rainfall estimates from TMPA 3B42 Version 7 to a ground-based gridded rainfall and found an index of agreement (d_r) ranging from ~ 0.65 to ~ 0.8 within the study area.

Ground-based rainfall data (P_{Obs}) from ~ 1270 gauges (Fig. S3) for the period 1995-2013 were interpolated to a 0.25° x 0.25° horizontal grid by Xavier et al. (2015). The rain gauge data were provided by the National Institute of Meteorology (Instituto Nacional de Meteorologia - INMET), the Water and Electric Energy Department of Sao Paulo state (Departamento de Águas e Energia Elétrica do Estado de São Paulo - DAEE) and ANA.

Two ET datasets were used in this study. For the period from 1995 to 2006, we used the evapotranspiration data from a global evapotranspiration algorithm (ET_{Glob}) developed by Zhang et al. (2010). The ET_{Glob} algorithm applies the Priestley-Taylor method to quantify open water evaporation and a modified Penman-Monteith method to quantify canopy transpiration and soil evaporation (Zhang et al., 2010). It uses Normalized Difference Vegetation Index (NDVI) to derive biome-specific canopy conductance values. The input data used to calculate ET_{Glob} are daily meteorology from NCEP/NCAR (National Center for Atmospheric Research) reanalysis data, NDVI from the AVHRR (Advanced Very High Resolution Radiometer) GIMMS (Global Inventory Modeling and Mapping Studies) , and solar radiation from NASA's GEWEX (Global Energy and Water Exchanges) Surface Radiation Budget Release 3.0 (Zhang et al., 2010). To parameterize the NDVI-based conductance model, measurements of 34 representative FLUXNET towers of major global vegetation types were used. Then, 48 additional independent towers were used to validate the ET_{Glob} algorithm (Zhang et al., 2010). According to Zhang et al. (2010), monthly estimates from ET_{Glob} showed good agreement ($0.8 \leq R^2 \leq 0.84$) with observed tower fluxes located

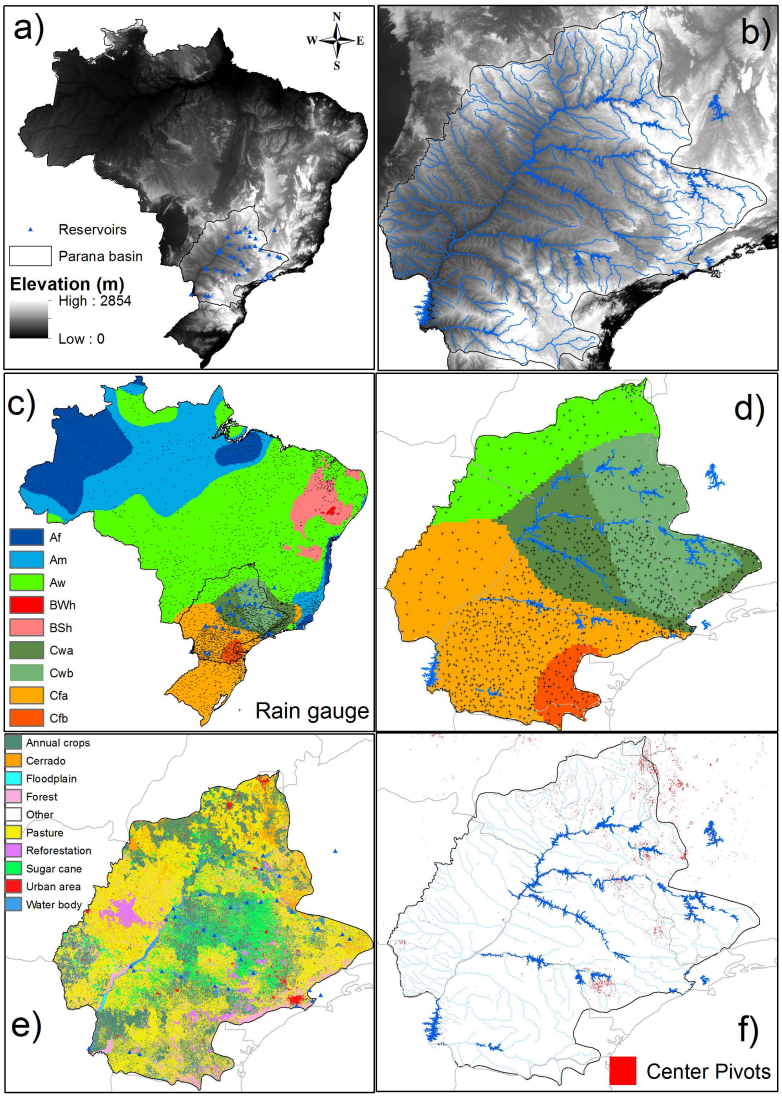

Figure S3. Elevation map of Brazil (a) and of Paraná basin (b); updated version of Koppen-Geiger climate classification of Brazil (c) and PB (d); land use map of PB (e); map of PB and center pivots. Climate classification: Af: Tropical rainforest, Am: tropical monsoon, Aw: tropical wet and dry (savanna climate), BWh: hot desert, BSh: hot steppe climate (semi-arid), Cwa: humid subtropical with dry winter, Cwb: temperate highland tropical with dry winters, Cfa: humid subtropical with hot summer, Cfb: maritime temperate with warm summer.

in representative land cover types globally. The ET_{Glob} outputs are available in a 8 km resolution grid globally.

For an overlapping period of six years (2000-2006) and the remaining period (until 2010), ET estimates based on MODIS (MODerate resolution Imaging Spectroradiometer) satellite were used. The MOD16 algorithm (Mu et al., 2007, 2011) combines information of land cover, albedo LAI (Leaf Area Index), EVI (Enhenced Vegetation Index) retrieved from MODIS with daily meteorological reanalysis data from NASA's Global Modelling and Assimilation Office (GMAO) to derive 8-day ET based on Penman-Monteith equation in a regular 1 km-horizontal resolution grid. MOD16 is an improved version of the previous ET algorithm developed by (Mu et al., 2007) in which the following improvements are highlighted by Mu et al. (2011): (i) simplification of the vegetation cover fraction calculation; (ii) ET is calculated as the sum of daytime and nighttime components; (iii) a soil heat flux calculation was added; (iv) improved estimates of stomatal conductance, aerodynamic and boundary layer resistances; (v) separation between dry and wet canopy surfaces; and (vi) creation of moist and saturated wet surfaces from the previous single soil surface.

Table S2. General information of the analyzed reservoirs

ID	Hydroelectric Plant	Latitude	Longitude	State	Area (km^2)	Vol (hm^3)
R1	Agua Vermelha	-19.86	-50.34	MG	647	16883
R2	Bariri	-22.15	-48.75	SP	45	1089
R3	Barra Bonita	-22.64	-48.27	SP	310	4191
R4	Billings	-23.79	-46.57	SP	88	995
R5	Cachoeira Dourada	-18.5	-49.49	MG	59	523
R6	Camargos	-21.33	-44.62	MG	60	792
R37	Cantareira System	-	-	SP	86	990
R8	Chavantes	-23.13	-49.73	SP	363	8795
R7	Capivara	-22.8	-51.04	SP	564	10541
R9	Corumbá I	-17.99	-48.53	GO	44	1030
R10	Emborcação	-18.44	-47.99	GO	382	17725
R12	Furnas	-20.96	-45.85	MG	1203	22950
R11	Funil	-21.16	-44.9	MG	31	541
R14	Ibitinga	-21.76	-48.99	SP	92	981
R15	Itaipu	-25.41	-54.59	PR	1338	29000
R13	Ilha Solteira	-20.38	-51.36	MS	1165	21060
R16	Itumbiara	-18.41	-49.1	MG	702	17000
R17	Jaguará	-20.02	-47.43	MG	33	460
R19	Jupiá	-20.78	-51.63	MS	297	3353
R18	Jaguari	-23.19	-46.08	SP	38	1236
R20	Jurumirim	-23.21	-49.23	SP	414	7008
R21	Marechal Mascarenhas de Moraes	-20.42	-46.85	MG	233	4040
R22	Marimbondo	-20.31	-49.19	SP	363	6150
R23	Miranda	-18.91	-48.04	MG	46	1120
R24	Nova Avanhandava	-21.12	-50.2	SP	195	2775
R25	Nova Ponte	-19.16	-47.36	MG	406	12792
R27	Paraibuna	-23.37	-45.66	SP	132	4732
R26	Porto Colômbia	-22.44	-52.97	MS	128	2335
R28	Promissão	-21.3	-49.78	SP	519	7759
R29	Rosana	-22.59	-52.86	SP	196	1912
R30	Salto Osŕio	-25.53	-53.01	PR	47	1124
R31	Salto Santiago	-25.61	-52.62	PR	192	6756
R32	Sao Simão	-19.02	-50.5	GO	609	12540
R36	Taquaraçu	-22.62	-51.78	SP	85	674
R33	Três Irmãos	-20.67	-51.3	SP	651	13373
R34	Três Marias	-18.21	-45.26	MG	856	23778
R35	Volta Grande	-20.09	-48.04	MG	182	4220

Vol = Total Volume capacity (1000 hm^3 = $1km^3$)

The algorithm was validated by comparing global ET estimates against measurements from 46 eddy flux towers, being found mean absolute bias of daily ET of ~ 0.33 mm day^{-1} (Mu et al., 2011). A regional evaluation inside Paraná basin of MOD16 ET estimates (ET_{MOD}) was reported by Ruhoff et al. (2013). Their analysis comprised a local and regional scale comparison between the remotely sensed energy fluxes and that derived from eddy covariance measurements and from a hydrological model (MGB-IPH). The flux towers are located at two sites within the Rio Grande basin in areas of sugar cane and pasture, respectively. Their findings show a good correlation (~ 0.8) between the 8-day averaged ET_{MOD} and flux tower data. However, the annual ET at local scale was ~ 20 % overestimated by MOD16 in the pasture area and, at basin scale, the average annual ET from MOD16 was ~ 20 % lower than those derived from the MGB-IPH model (Ruhoff et al., 2013).

S3.4 GRACE data

The GRACE-based monthly time variable gravity (TVG) fields used in this study are the latest release (RL05), generated as spherical harmonic (SH) Stokes coefficients up to degree and order 60 released by the Center of Space Research (CSR) of the University of Texas at Austin. The time span considered is from 04/2002 through 04/2015. Numerical model-based atmospheric and oceanic mass redistribution

and tidal effects were removed for de-aliasing prior to analysis. Anomalous fields in SH format were obtained by removing a static field (GGM05S), thus GRACE TVG over land should reflect primarily changes in TWS, and other unmodeled geophysical signals such as postglacial rebound (PGR) or tectonic mass transports.

GRACE TVG fields are plagued with strong noises, presenting North-South stripe and increased errors in high degree and order SH coefficients. Following filtering method adopted by Zhang et al. (2015), we use the de-correlation filter Swenson and Wahr (2006) to suppress stripes and fan filter with (Zhang et al., 2009) spatial resolution of 250 km to work on noises. The degree 2 order 0 (C20) coefficient is replaced by higher quality satellite laser ranging solutions (Cheng et al., 2011). The PGR effect is removed using model outputs further (A et al., 2012). Filtered monthly TVG fields in SH format are converted to gridded $1^\circ \times 1^\circ$ solutions to match outputs from land surface models spatially.

S4 Methods

S4.1 Test statistics

The non-parametric Mann-Whitney U-test (Mann and Whitney, 1947) is a common alternative to the parametric Student's t-test for testing whether two independent samples, X and Y, come from the same population. It is equivalent to the Wilcoxon rank-sum test or Wilcoxon-Mann-Whitney rank-sum test and consists of calculating the statistic U (Eq. 1), which is the number of times an element y precedes an element x when X and Y are sorted in ascending order.

$$U_S = W - \frac{N_S(N_S+1)}{2} \tag{1}$$

Where U_S is the lesser of U_X and U_Y, W is the sum of the ranks in each sample, N_S is size of sample S (X or Y). If the null hypothesis (H_0) that the two samples come from the same population is rejected, it means that X and Y are statistically different from each other. Here, X represents the reservoir(s) mean storage at various time scales for each water year (WY) tested and Y is the mean monthly storage for the entire period less the tested one. We tested H_0 using the seasonal mean (March-April-May) at 5 % significance level.

S4.2 Trend analysis - Mann-Kendall

As noted by Cox and Stuart (1955), time series with positive serial correlation (such as most of hydrological variables) may increase the chance of trend detection even in the absence of a real trend. To avoid that, the serial correlation should be removed (pre-whitening) prior to applying the test or the test should be modified to account for serial correlation (Hamed, 2008). Although the first option has been widely adopted (Gao et al., 2011; Burn and Hag Elnur, 2002; Zhang et al., 2001), it is not suitable if the time series is not a autoregressive model AR(1) such as the analyzed data here. In such cases, the pre-whitening process is insufficient (Storch, 1999). In other cases, pre-whitening cannot improved trend identification as it may weaken trend's magnitude (Sang et al., 2014). Hence, we adopted the modified Mann-Kendall trend test for seasonal data with serial correlation proposed by (Hirsch and Slack, 1984). The Mann-Kendall test statistic (S) is given by:

$$S = \sum_{i<j} \mathrm{sng}(x_j - xi) \tag{2}$$

Where x_i are the observations of the time series X; $\mathrm{sng}(x) = -1$ if $x_j < x_j$; $\mathrm{sng}(x) = 0$ if $x_j = x_j$ and $\mathrm{sng}(x) = 1$ if $x_j > x_j$. The significance of the trend is tested by comparing the test statistic Z_S (Eq.) with a certain significance level α (Kendall, 1975).

$$Z_S = \begin{cases} (S-1)/\sqrt{\mathrm{VAR}(S)} \text{ if } S > 0 \\ 0 \text{ if } S = 0 \\ (S+1)/\sqrt{\mathrm{VAR}(S)} \text{ if } S < 0 \end{cases} \tag{3}$$

Where, Var(S) is the variance of S. If $|Z_S| < Z_\alpha$, no trend was detected. In the modified version, the test is performed individually for each season (in this study, months) and H_0 is tested only if all seasons have the same direction.

S4.3 Drought indices

The Standardized Precipitation Index was selected as the meteorological drought index because it is probabilistic, its implementation is relatively simple, and its interpretation is spatially invariant (Guttman, 1998). SPI is a common choice for monitoring wetness and dry conditions over a region (Vicente-Serrano and López-Moreno, 2005; Fiorillo and Guadagno, 2009).

SPI uses historical rainfall data to determine, at different timescales, the periods of positive and negative anomalies in rainfall based on the cumulative probability of rainfall occurrence over an area or at point (McKee et al., 1993). The gamma probability function is frequently chosen for describing the rainfall over an area (Teodoro et al., 2015), hence it was used in this study for fitting the rainfall data relative to a 35-year time span (1980-2015).

The Streamflow Drought Index (SDI) (Nalbantis and Tsakiris, 2008) was used for characterizing hydrologic drought events in the study area. This index is analogous to SPI in that it is computationally inexpensive, easy to implement, and reduces the drought characterization to a simple severity versus frequency relationship (Nalbantis and Tsakiris, 2008). In addition, it is not data demanding as it requires only streamflow data. SDI is defined for each i-th hy-

drological year and k-th reference period, with k=1 for Sep-Jan, k=2 for Sep-Apr, k=3 for Sep-Jul and k=4 for Sep-Aug.

$$SDI_{i,k} = \frac{V_{i,k} - V_k}{\sigma_k} \quad (4)$$

where $V_{i,k} = \sum_{j=1}^{3k} Q_{i,j}$ is the cumulative streamflow volume, with $i = 1, 2, ...;\ j = 1, 2, ...;\ k = 1, 2, 3, 4$. $\overline{V_k}$ and σ_k are the mean and standard deviation of the cumulative streamflow volumes.

There are several reservoirs along the mainstream which implies that the inflow to downstream reservoir is the combination of its own (exclusive) contributing basin (hereafter named undisturbed basin - UB) to and the outflow from an upstream reservoir (UR). Thus, for most of the analyzed reservoirs, SDI does not reflect solely the natural drought condition but to which degree of drought condition the observed inflow is relative to. Discharge records from the dams were available only after 1995-2015. A SDI calculated considering a longer time period ($\geq$ 30 years) would better identify the events of hydrological drought. The reader should be aware that the results for SDI indicate the occurrence of dry periods relative to a 20-year window.

S4.4 Cluster Analysis

Cluster analysis can be very useful for identifying distinct patterns among large samples. There are several techniques of data clustering in which distinct criteria are used to group the data, usually involving some type of similarity. An approach commonly adopted to identify similar groups among hydrological time series (Brito Neto et al., 2015; Gong and Richman, 1995) is the hierarchical clustering; in which the similarities among elements is measured by a distance function (Bailey, 1994). The distance between pairs of elements (objects) will define the first clusters of the hierarchical tree (Fig S4). Then, the distance between clusters is computed and new cluster of higher hierarchy are formed and so on until there are only two groups. The hierarchy of the clusters can be easily represented through a dendrogram (Fig. S4), where the distance between objects (or clusters) is represented in the Y-axis.

Two decisions that need to be made to compute the clusters are: which distance function will be used and which linkage criterion. In this study, Ward's method (Ward, 1963) was selected as linkage criterion. This method uses a minimum variance algorithm to compute inner squared distance between two objects (a, b) (Eq. 5) (Ward, 1963). Among the distance functions available in Matlab, one popular choice that usually give good results (Ramoni et al., 2002) is the Euclidean distance ($\|\overline{x_a} - \overline{x_b}\|_2$).

$$d(a,b) = \sqrt{\frac{2n_a n_b}{(n_a + n_b}} \|\overline{x_a} - \overline{x_b}\|_2 \quad (5)$$

In this study, the so called objects used to generate the clusters are time series of monthly storage. Because some of these signals contain significant noise that can disrupt the clustering algorithm, it is useful to reduce the noise prior to computing the clusters. To this end, the use of a wavelet-denoising approach is a better option compared to other classical methods, such as Fourier Analysis (Chou, 2011).

The signal decomposition is achieved by applying a Discrete Wavelet Transform (DWT), which consist of a digital filtering process through time-domain that allows high and low frequencies to be separated from the original signal. In this process, two complementary filters (low pass, h[.], and high pass filter, g[.]) are applied to the original signal, resulting in two signals for each level: Approximations (APP) and Details (DET). The APP contains the high-frequency components of the signal and DET the low-frequency components. The h[.] and g[.] filters are the only elements necessary to calculate a DWT of a signal.

These filters are defined according to the chosen mother wavelet (ψ) which, in turn, depends on the data being analyzed. A common choice in many hydrologic studies is the Daubechies wavelet transform (Ramana et al., 2013; Nalley et al., 2012; Wei et al., 2012) because of its ability for denoising singals and its intrinsic features that make it capable of localizing events in time-dependent signals (Popivanov and Miller, 2002; Vonesch et al., 2007). Following the choice of past studies (Nalley et al., 2012; Wei et al., 2012), we used the Daubechies wavelet with order N=5 (db5) to decompose the signals (Fig. S5). Based on the number of vanishing moments (ν) of db5 and the number of data points (n), the maximum decomposition level (L) is 5 (de Artigas et al., 2006), thus, we adopted L= 5. We used the Multilevel 1-D wavelet decomposition function from the Matlab Wavelet Toolbox to perform the DWT of the signals of monthly storage time series.

S5 Results

S5.1 Trends in TWS and SMS

The trends in GRACE TWS and soil moisture storage (SMS) are shown in Fig. S6. Between Apr 2002 and Jan 2011, GRACE TWS shows a faster recovery ($0.97\,\mathrm{cm\,yr^{-1}}$) compared to that in SM ($0.23\,\mathrm{cm\,yr^{-1}}$). After 2010/2011 both signals show a negative trend but GRACE TWS responds faster ($-4.2\,\mathrm{cm\,yr^{-1}}$) to the dry conditions than the SM signal ($-1.34\,\mathrm{cm\,yr^{-1}}$).

Groundwater data (Fig. suggest that the discrepancy between TWS and SMS+RESS shown in the manuscript, Fig. 5, may be related to depletion in deep SMS or groundwater storage.

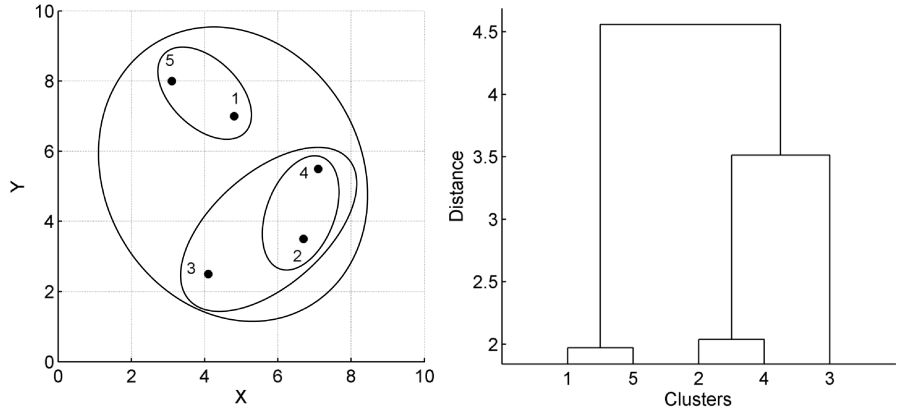

Figure S4. Example of the clustering of 5 random elements and the resulting hierarchical tree.

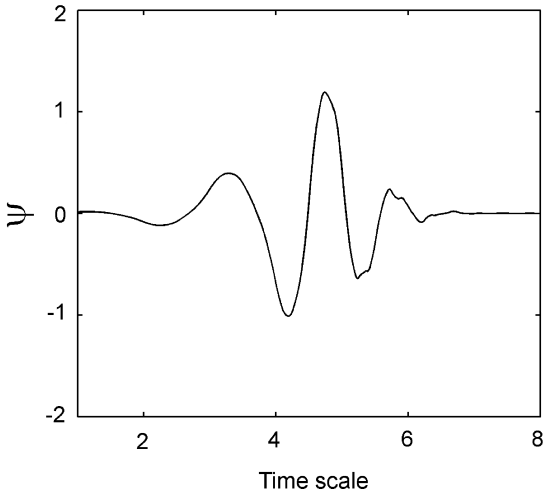

Figure S5. Daubechies wavelet with order 5 (db5)

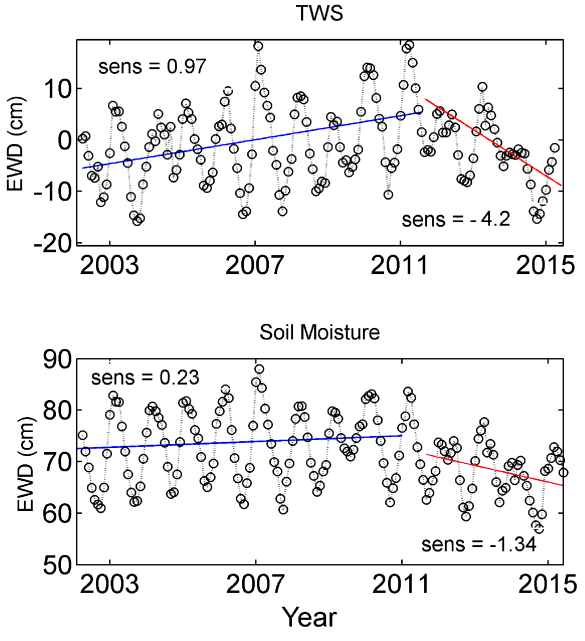

Figure S6. Trends in TWS and soil moisture

S5.2 Analysis of ET

ET estimates show that the seasonal signal of $\mathrm{ET_{MOD}}$ has a larger variation range than $\mathrm{ET_{Glob}}$, although both datasets presented similar estimates of maximum rates (Fig. S8). Given the uncertainty involved in such estimates, no attempt is made to identify whether $\mathrm{ET_{Glob}}$ overestimates the minimums or $\mathrm{ET_{MOD}}$ underestimates them, rather we analyze the changes in the ET signal.

The increased ET was observed in most of the Paraná basin, especially over the contributing areas of the majority of the analyzed reservoirs. Between 1995 and 2006, both signals ($\mathrm{ET_{Glob}}$ and $\mathrm{ET_{MOD}}$) are practically invariant although the moving average lines show that higher $\mathrm{ET_{MOD}}$ is $\sim 25\,\%$ higher than $\mathrm{ET_{Glob}}$ estimates.

The low magnitude of such change may not significant, given the uncertainties in ET, which vary according to vegetation type: $\pm 4\,\%$ (savanna), $\pm 5\,\%$ (tropical forest) and $\pm 13\,\%$ (pasture/agriculture) (Loarie et al., 2011; Rudorff et al., 2010). The spatial change of mean annual ET (dET) between these two periods (2000-06 and 2007-2014) is shown in Fig. S9. The increased ET was observed in most of the Paraná basin, especially over the contributing areas of the majority of the analyzed reservoirs. A possible explanation for that would be the expansion of sugar cane. It has been shown that the replacement of pasture by sugar cane in the Cerrado increases ET (Loarie et al., 2011) and the São Paulo ($\sim 30\,\%$ of Paraná basin) is the largest sugar cane producer in Brazil, being responsible for $\sim 60\,\%$ of the national production (Rudorff et al., 2010). More than half of Cerrado areas in

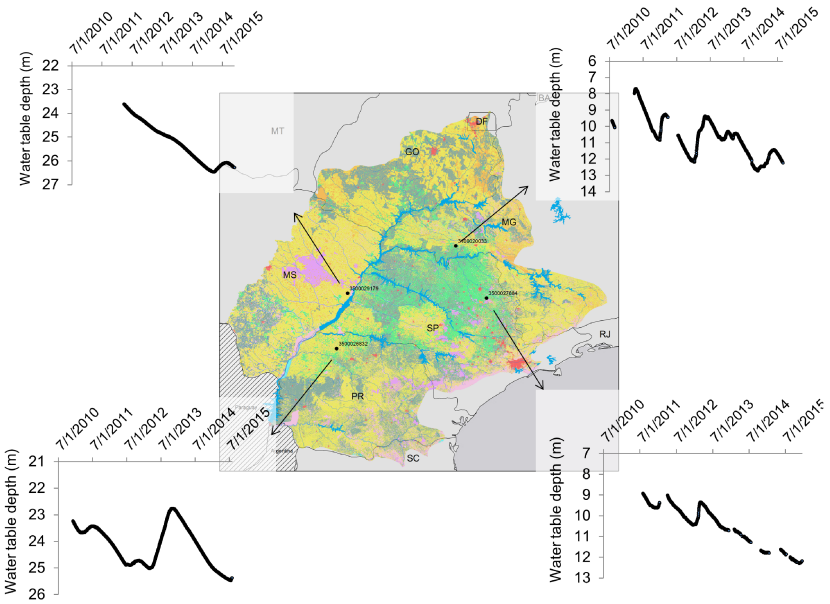

Figure S7. Typical time series of groundwater levels between 2010 and 2015 in the Paraná Basin

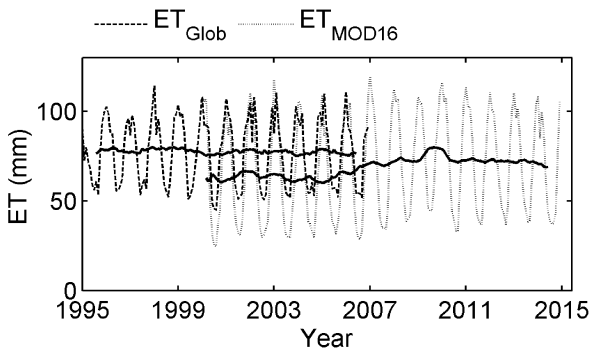

Figure S8. Time series of $\mathrm{ET_{Glob}}$ and $\mathrm{ET_{MOD}}$

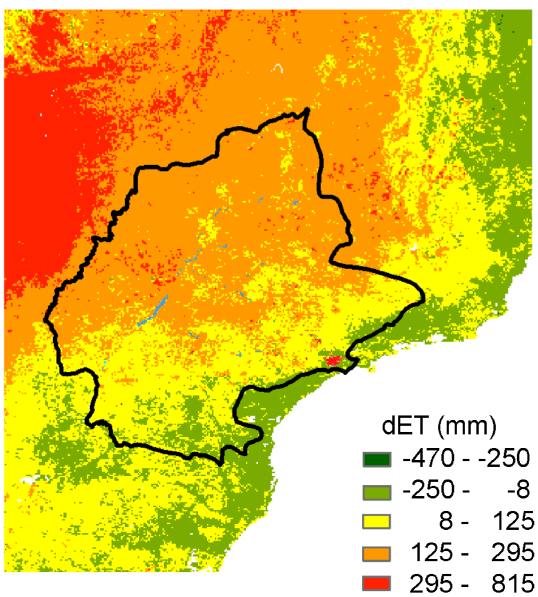

Figure S9. Spatial changes in annual ET averaged from 2000 to 2006 and 2007 to 2014

SP are now sugar cane plantings. However, the comparison between the ET change map and land use map show that the higher changes in ET (>125 mm $\mathrm{yr^{-1}}$) occurred mostly in areas with annual crops and pasture while the areas preponderantly occupied by sugar cane had an increase in annual ET of $\sim$ 0-125 mm $\mathrm{mo^{-1}}$.

The average temperature in the Paraná basin has decrease $\sim 0.04\,^{\circ}\mathrm{C\,yr^{-1}}$ in the past 20 years but (Fig S10).

S5.3 Trends in RESS

Fig. S11 shows the positive/negative trends in total reservoir storage (RESS) during recovery/depletion periods since 1995.

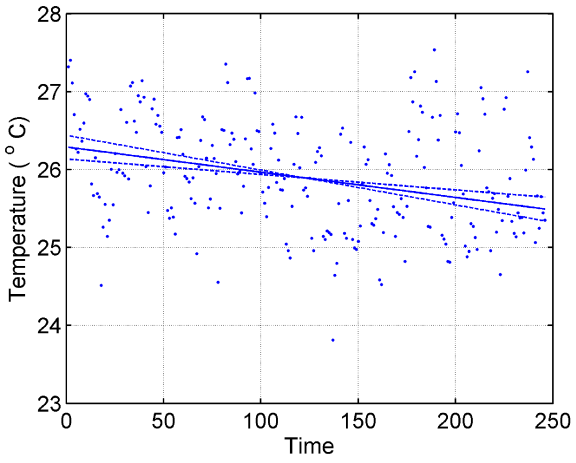

Figure S10. Long-term trend in temperature (1995-2015)

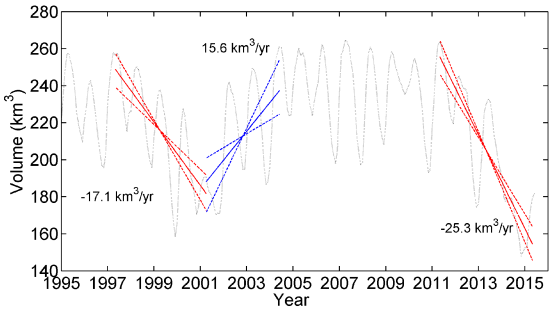

Figure S11. Trends in reservoir storage

S5.4 Cluster analysis

To determine the cluster, the user can either set a desired number of clusters or optimize this number based on link consistency. In the first option, the maximum within-cluster distance is determined in order to form a pre-defined number of cluster whereas in the second approach, the distance is gradually reduced seeking to form clusters whose links have approximately the same height as the links below it. Note that the quality of the clustering analysis depends on the data itself, that is, if the sample is too heterogeneous the distance among clusters will be mostly large, reducing consistency and the feasibility of such method. In other words, some data cannot be grouped because there are not enough similarities among the samples.

Here, the reservoirs were clustered in six groups (G1, G2,..., G6) based on the time series signal of monthly storage. The hierarchical tree showing the groups and the linkages between them is illustrated by the dendrogram in Fig S12. It is easy to visualize how the groups relate to each other and how the maximum cluster distance (MCD) controls the definition of the groups. The two main features intended to

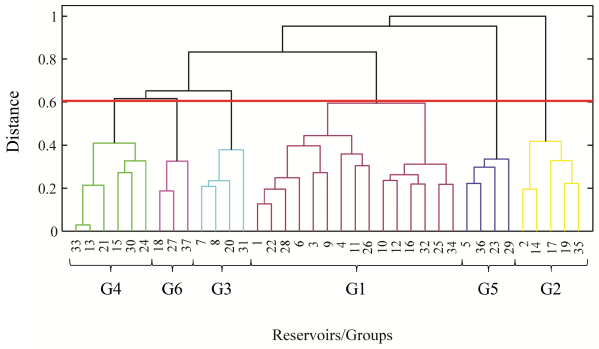

Figure S12. Dendrogram plot showing the hierachical cluster tree. The distance between individual clusters is given by the height of links. The red horizontal line shows the maximum cluster distance used to determine the clusters

be highlighted by creating those clusters are: seasonality and changes in time.

Although the dendrogram in Figure S12 may suggest higher link consistency for MCD ~ 0.5, the similar seasonal signal characteristic of G1 would be present in the new groups formed from G1 would show. For this reason, the configuration in Fig S12 was maintained.

The inconvenience of such choice relies on the fact that the distance between the two main clusters in G1 (G1.1 and G1.2) is almost the same as that between G4 and G6. However, the comparison between G4 and G6 from Fig. 6 (manuscript) and G1.1 and G1.2 from Fig. S13 reveals that the main differences between the objects in G4 and G6 are mostly related to the timing and magnitude of changes while G1.1 and G1.2 differ in terms of sensitivity to changes. This can be exemplified by how the storage varies in the years that follows the 2000/2001 (black dashed circles) and 2013/2014 (green dashed circles) droughts. Note that after the 2013/2014, the reservoirs in G1.1 show a rapid recover compared to those in G1.2.

S5.5 Spatial analysis of reservoir depletion/recovery

Given the large extension of our study area, it is expected to identify different responses of reservoir storage change to climatic variations. In order to assess such responses to the two main droughts that occurred in the Paraná basin since 1995, we performed a trend analysis using storage data of each reservoir. The following periods were considered: May 1997 - Apr 2001, Apr 2001- Jun 2004 and May 2011 - May 2015. The results showing depletion/recovery of each reservoir is shown in Figs. S14-S16 and in Table S3. During the first period (1997-2001), most of the reservoirs depleted, especially those with larger dimensions. Between 2001 and 2004, only a few reservoirs continued to deplete, including all of those in the Paranapanema sub-basin. Comparing Figs. S14 and S16 it becomes evident the greater impacts of the

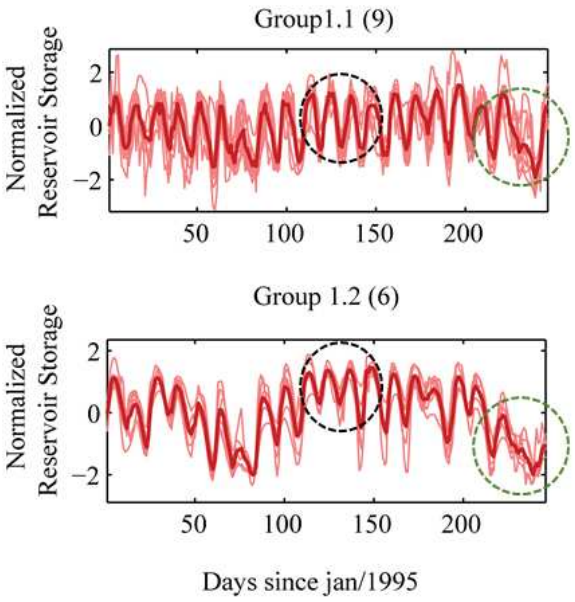

Figure S13. Subdivision of group 1 in two clusters

2013/2014 drought compared to that in 2000/2001. Between 1997 and 2001, only one reservoir had a drastic depletion of more than 75 % (red). Between 2011 and 2015, it can be seen a large number of cases that depleted more than 50 %. Only one reservoir had an increase (0 - 25 %) of storage during that last period.

S5.6 Spatial analysis of precipitation anomaly

The distinct responses shown in Section S5.5 are, in part, explained by the spatial patterns of precipitation that occurs in the study area. Fig. S17 shows maps of annual rainfall anomaly (P_{anom}) relative to the analyzed years in this study. As mentioned in the manuscript and showed in Fig. S16, one major reason for the depletion of a greater number of reservoirs during the 2014 drought is the greater extents of negative rainfall anomaly over PB, mainly in the mid-east part (Tietê and Rio Grande sub-basins) where a $\mathrm{P_{anom}} \sim -50\,\%$.

S5.7 Natural and human-controlled variables

The natural discharge was estimated as the difference between total inflow and outflow from the upstream reservoirs. The main limitation to such approach is that the available records of reservoirs outflow are in daily basis and, as the distance between upstream and downstream dams grows, the greater is the difference between the discharge registered on the upstream dam and the actual discharge arriving at the downstream reservoir. For example, there are ~ 190 km between the Marimbondo dam and Água Vermelha reservoir, which implies that there is actually no accurate data of how much of the total inflow in Água Vermelha corresponds to the outflow from Marimbondo. For those reservoirs located downstream to other dams, we applied the moving average of discharges (total inflow, outflow from upstream) to reduce the differences caused by such lag time and, then, estimate the natural component of the total inflow ($\mathrm{Q_{nat}}$). There were some situations in which we only analyzed the SDI relative to the total inflow: a significant difference between total inflow ($\mathrm{Q_{in}}$) and outflow from upstream ($\mathrm{Q_{up}}$) was detected; there is insufficient data to compute SDI relative $\mathrm{Q_{nat}}$; $\mathrm{Q_{in}} = \mathrm{Q_{nat}}$. The following figures are provided to complement the discussion provided in the Results section of the main manuscript. Plots of monthly storage, SPI, SDI or discharge are provided for 36 reservoirs and the Cantareira equivalent system.

Table S3. Summary of individual trend analysis of reservoir storage change

			Active Volume	% Total	Depletion/Recovery (km3)			Depletion/Recovery (% Act. Vol)		
Group	ID	Name	Capacity (km^3)	Capacity	May/97-Apr/01	Apr/01 -Jun/04	May/11-Apr/15	May/97-Apr/01	Apr/01 -Jun/04	May/11-Apr/15
1	R1	Água Vermelha	11.02	65%	-5.30	3.30	-6.88	-48%	30%	-62%
	R3	Barra Bonita	3.62	86%	-0.06	0.47	-0.33	-2%	13%	-9%
	R4	Billings	0.99	-		0.06	-0.17		6%	-17%
	R6	Camargos	0.67	85%	-0.23	0.18	-0.56	-34%	27%	-84%
	R9	Corumbá I	0.56	54%	-0.13	0.02	-0.05	-23%	4%	-8%
	R10	Emborcação	13.06	74%	-8.44	8.98	-7.18	-65%	69%	-55%
	R11	Funil	0.26	48%	-0.03	0.10	-0.11	-11%	40%	-41%
	R12	Furnas	17.22	75%	-13.01	11.78	-14.29	-76%	68%	-83%
	R16	Itumbiara	12.45	73%	-8.03	8.21	-6.68	-64%	66%	-54%
	R22	Marimbondo	5.26	86%	-3.05	1.76	-3.16	-58%	34%	-60%
	R25	Nova Ponte	10.38	81%	-7.35	4.66	-7.39	-71%	45%	-71%
	R26	Porto Colômbia	1.52	65%	0.00	0.33	-0.30	0%	22%	-20%
	R28	Promissão	2.48	32%	-0.45	0.24	-1.09	-18%	10%	-44%
	R32	São Simão	5.54	44%	-1.59	2.54	-3.35	-29%	46%	-60%
	R34	Três Marias	19.53	82%	-8.98	5.15	-18.90	-46%	26%	-97%
2	R2	Bariri	0.61	56%	0.02	0.01	-0.06	4%	1%	-10%
	R14	Ibitinga	0.05	5%	0.00	0.00	-0.01	10%	-2%	-29%
	R17	Jaguará	0.10	22%	-0.02	0.02	0.00	-24%	16%	-4%
	R19	Jupiá	0.90	27%	-0.01	0.04	0.00	-1%	5%	0%
	R35	Volta Grande	2.24	53%	-0.24	0.50	0.02	-11%	22%	1%
3	R7	Capivara	5.72	54%	-1.24	-1.00	-2.91	-22%	-18%	-51%
	R8	Chavantes	3.04	35%	-1.36	-0.63	-1.49	-45%	-21%	-49%
	R20	Jurumirim	3.16	45%	-1.87	-0.17	-1.48	-59%	-5%	-47%
	R31	Salto Santiago	4.09	61%	-0.63	-1.81	-0.39	-15%	-44%	-10%
4	R13	Ilha Solteira	5.52	26%	-2.32	2.33	-7.69	-42%	42%	-139%
	R15	Itaipú	19.00	66%	-0.51	0.34	-3.81	-3%	2%	-20%
	R21	M. M. Moraes	2.50	62%	-0.41	0.58	-0.78	-16%	23%	-31%
	R24	N. Avanhandava	0.43	15%	0.02	0.03	-0.16	4%	8%	-36%
	R30	Salto Osório	0.40	36%	-0.02	0.00	-0.01	-5%	1%	-2%
	R33	Três Irmãos	3.45	26%	-1.35	1.27	-4.32	-39%	37%	-125%
5	R5	Cachoeira Dourada	0.22	42%		-0.05	-0.01		-24%	-5%
	R23	Miranda	0.14	13%	0.00	-0.02	-0.01		-12%	-4%
	R29	Rosana	0.41	21%	-0.01	-0.03	0.03	-4%	-6%	6%
	R36	Taquaraçu	0.13	19%	0.00	0.00	0.00	-3%	-2%	-1%
6	R18	Jaguari	0.79	64%	-0.27	0.04	-0.76	-34%	5%	-96%
	R27	Paraibuna	2.63	56%	-1.06	-0.13	-2.29	-40%	-5%	-87%
	R37	Cantareira Syst.	0.99	-	-0.31	-0.18	-1.15	-31%	-18%	-116%

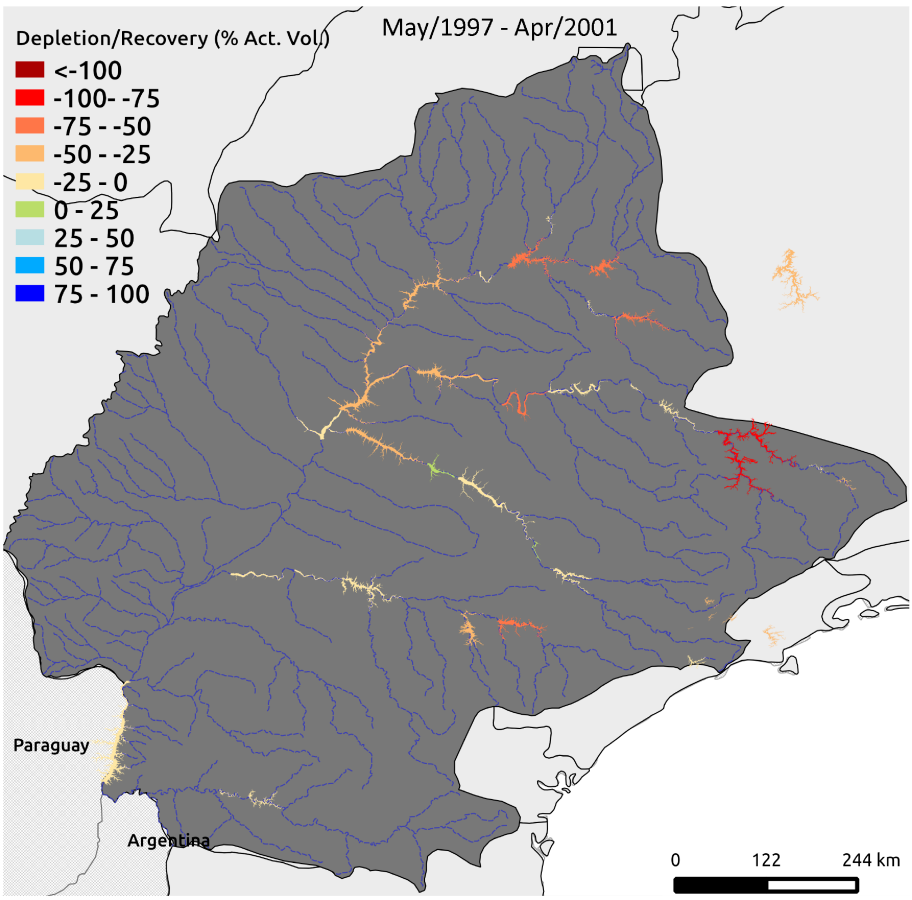

Figure S14. Trends in reservoir storage between May 1997 and Apr 2001

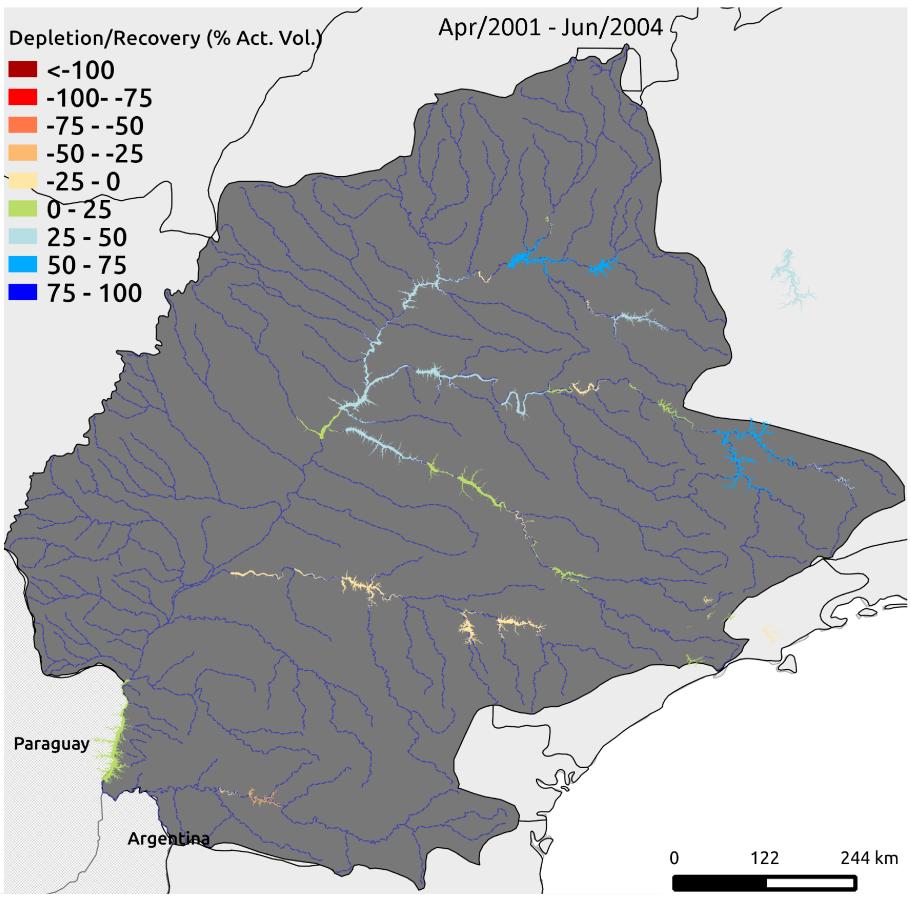

Figure S15. Trends in reservoir storage between Apr 2001 and Jun 2004

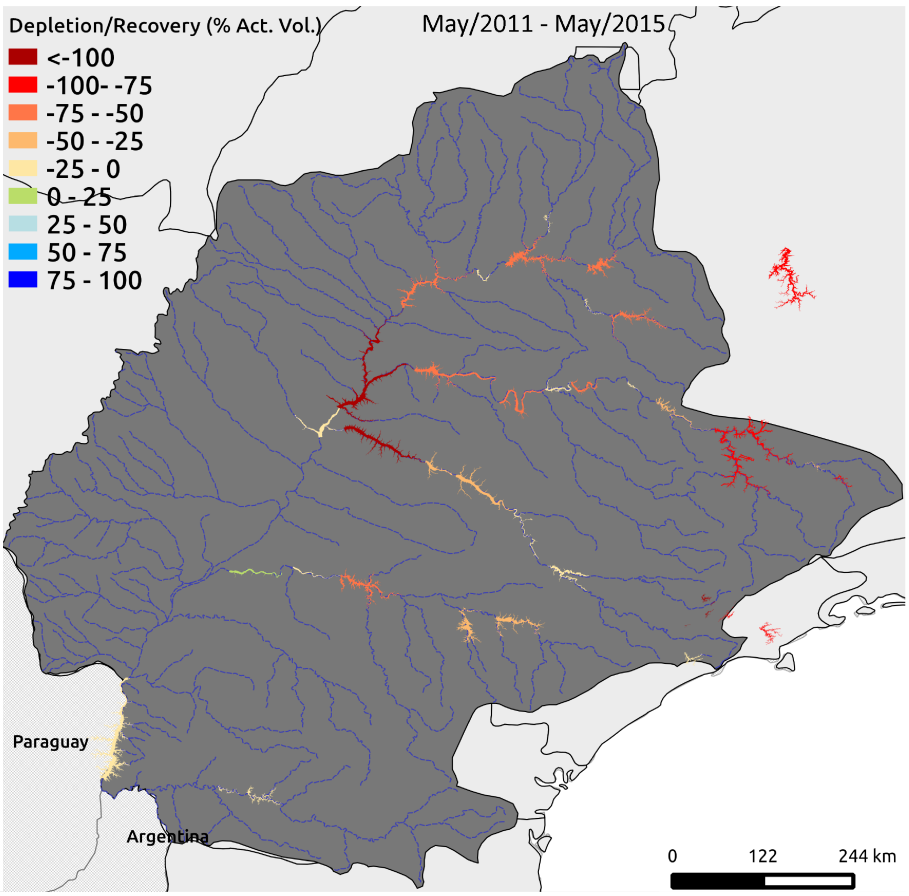

Figure S16. Trends in reservoir storage between May 2011 and M 2015

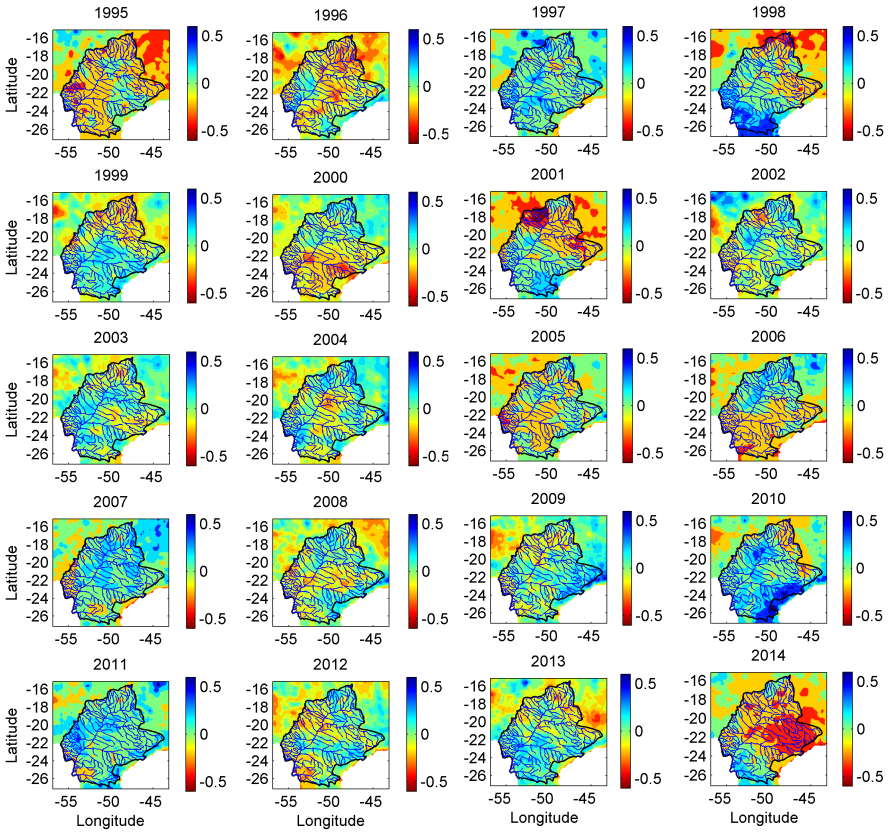

Figure S17. Maps of annual precipitation anomaly in Southeast Brazil from 1995 and 2015.

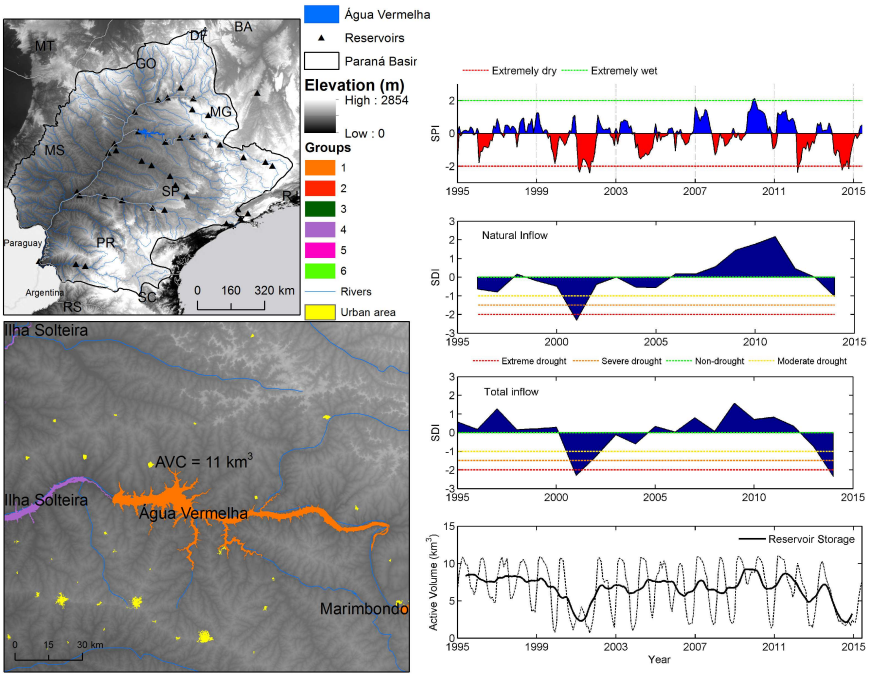

Figure S18. Time series of SDI, SPI and monthly storage: Água Vermelha Hydroelectric Plant (HEP)

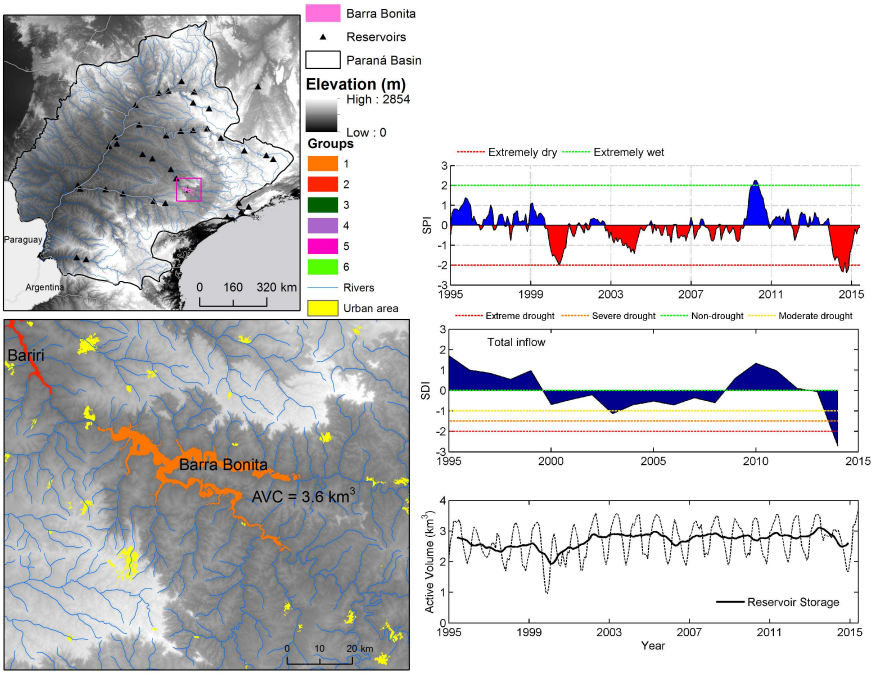

Figure S19. Time series of SDI, SPI and monthly storage: Barra Bonita HEP

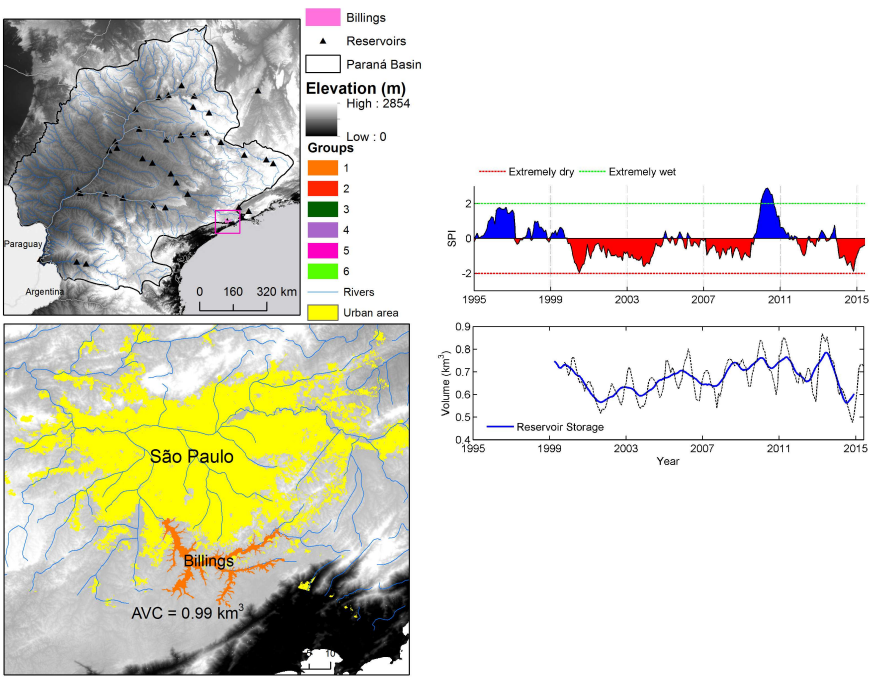

Figure S20. Time series of SDI, SPI and monthly storage: Billings

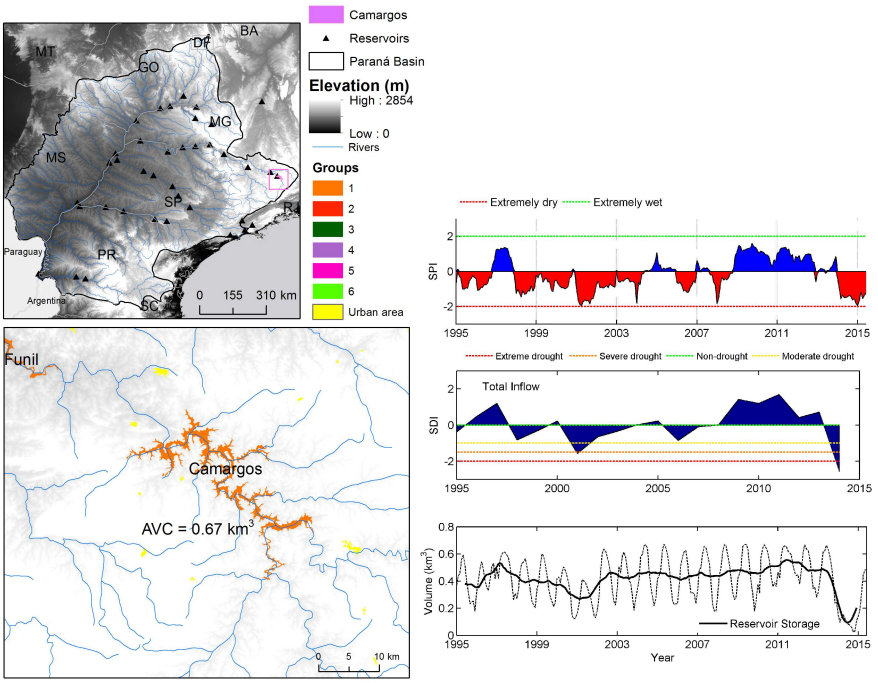

Figure S21. Time series of SDI, SPI and monthly storage: Camargos HEP

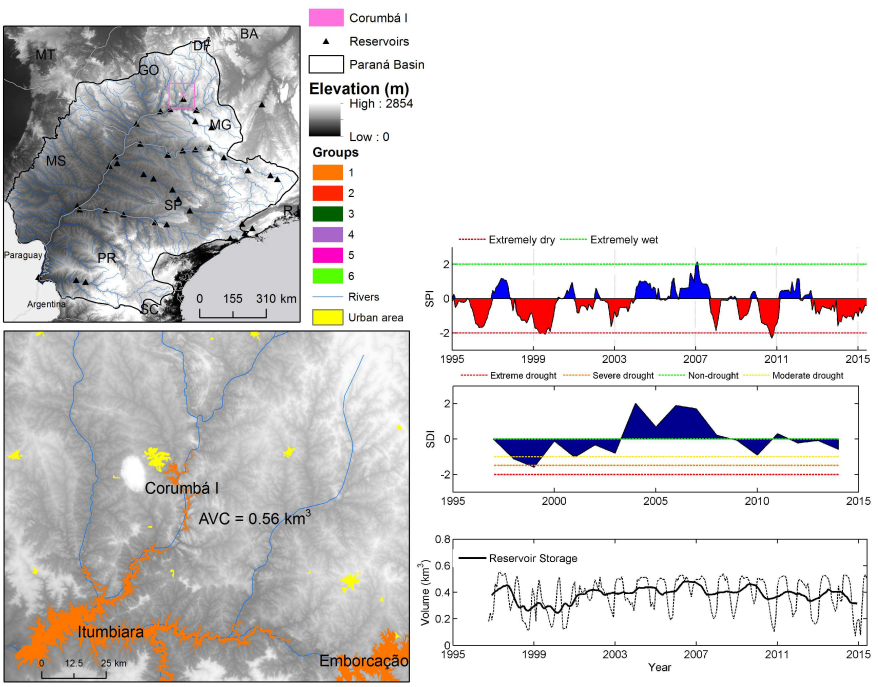

Figure S22. Time series of SDI, SPI and monthly storage: Corumbá I HEP

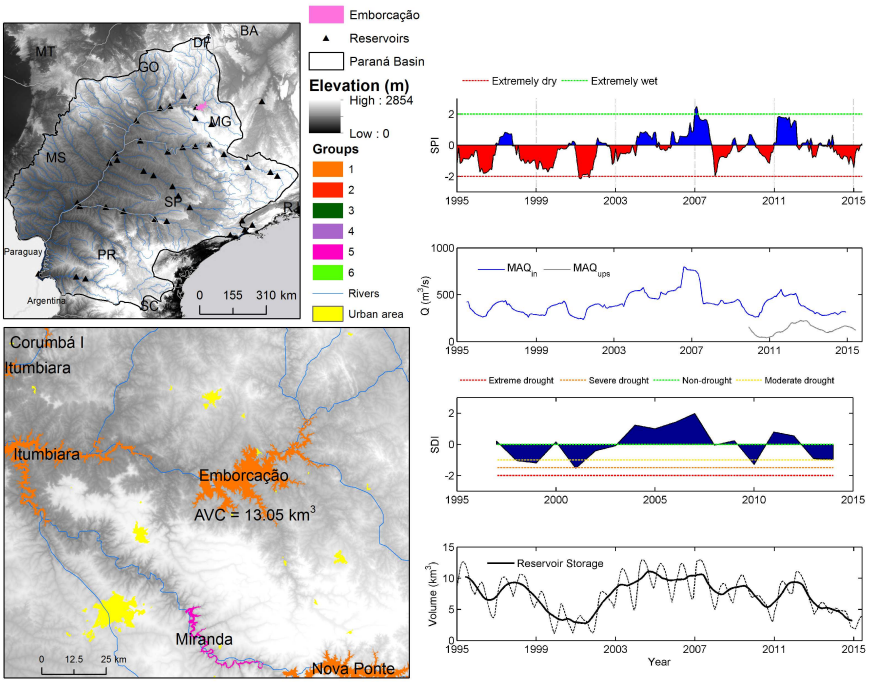

Figure S23. Time series of SDI, SPI and monthly storage: Emborcação HEP

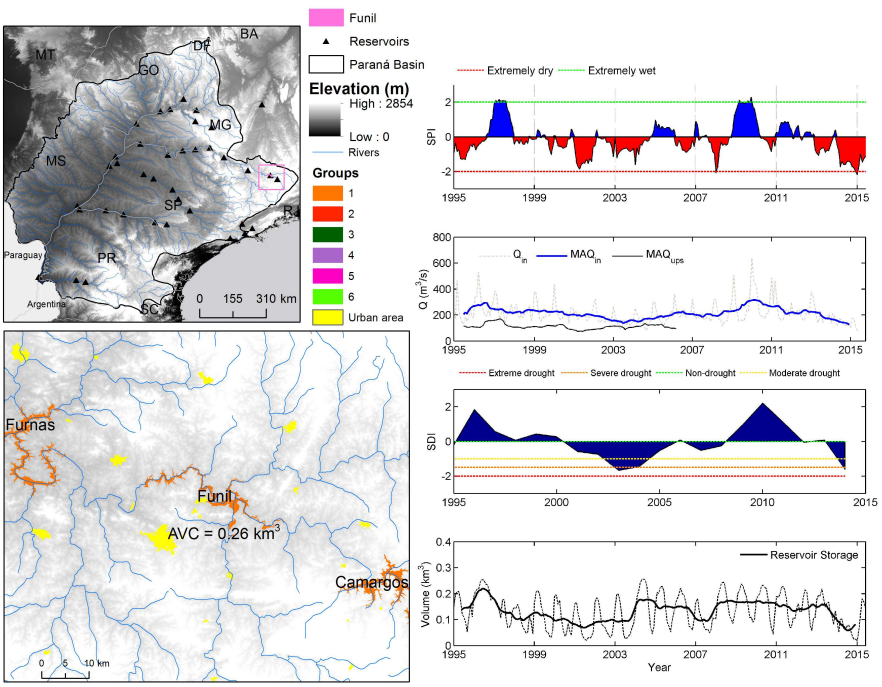

Figure S24. Time series of SDI, SPI and monthly storage: Funil HEP

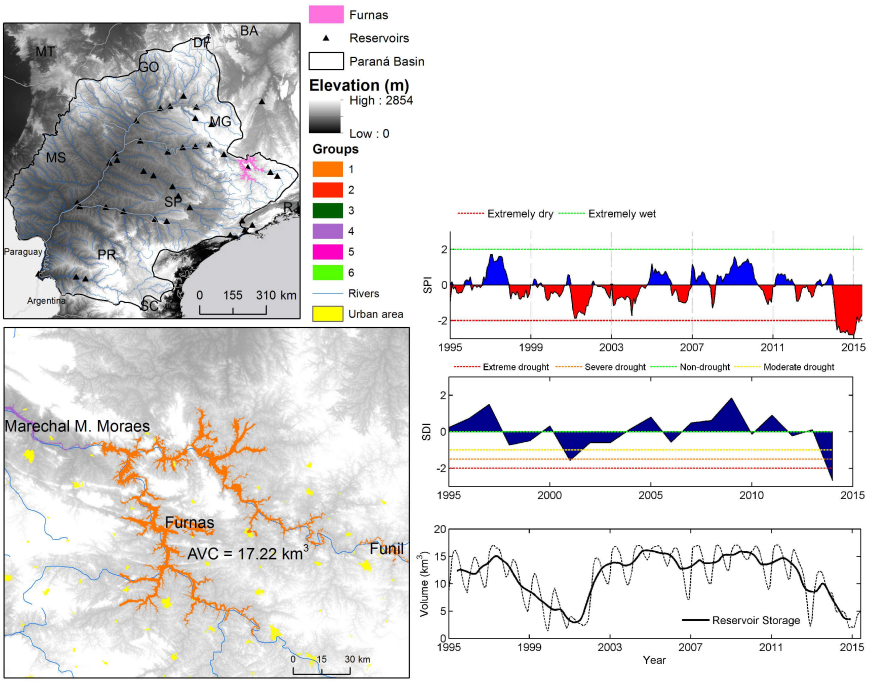

Figure S25. Time series of SDI, SPI and monthly storage: Furnas HEP

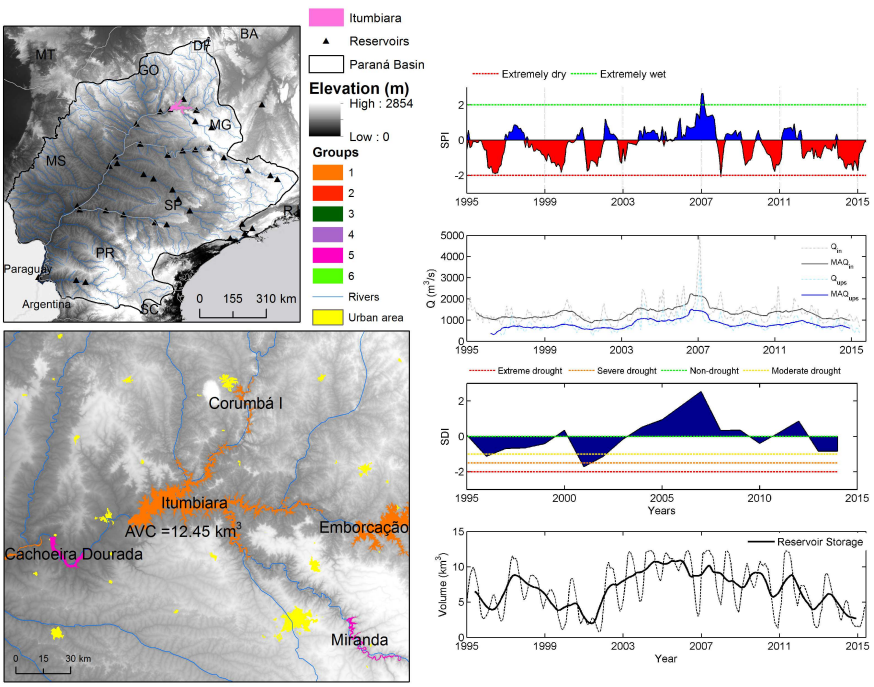

Figure S26. Time series of SDI, SPI and monthly storage: Itumbiara HEP

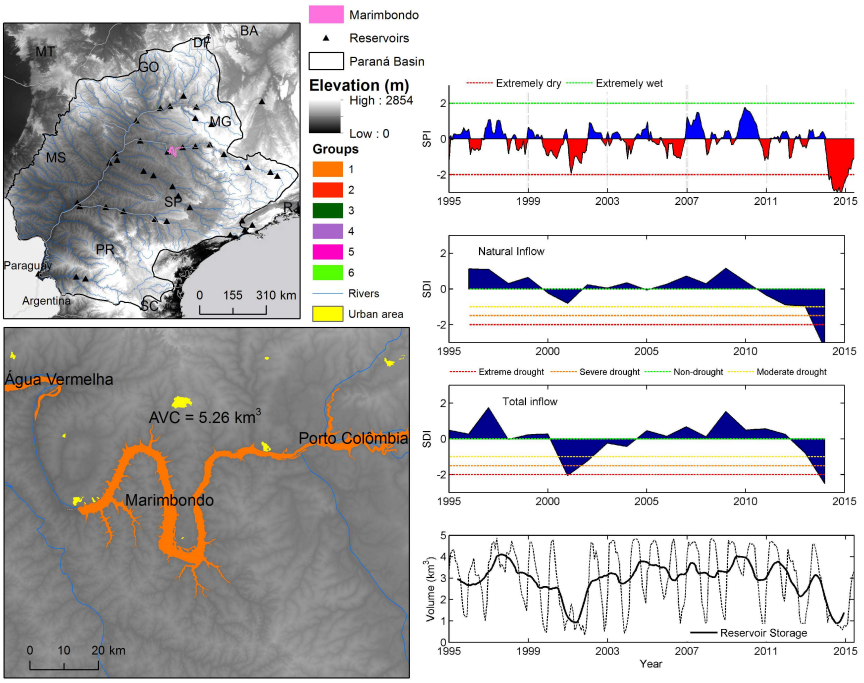

Figure S27. Time series of SDI, SPI and monthly storage: Marimbondo HEP

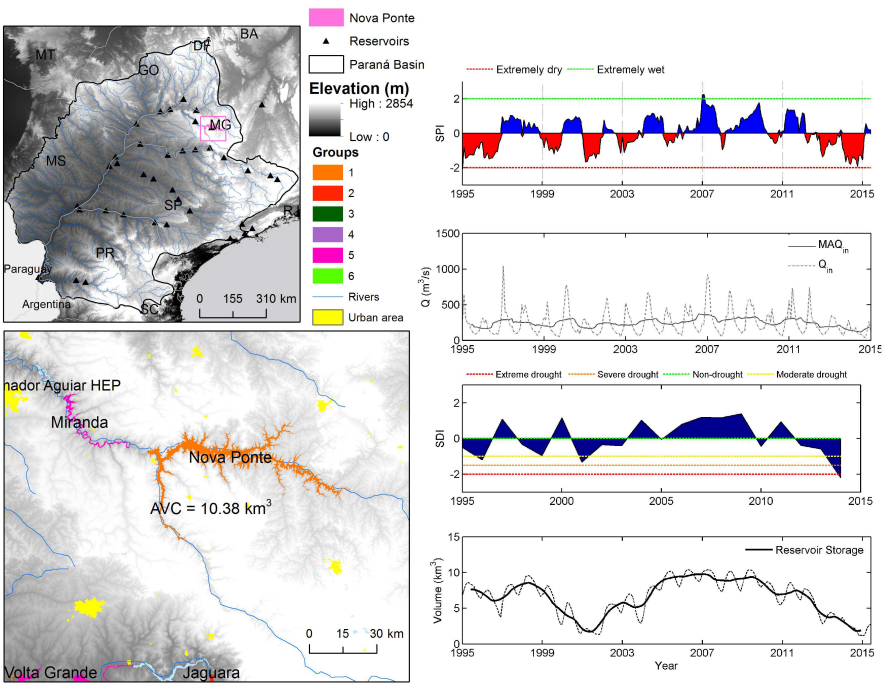

Figure S28. Time series of SDI, SPI and monthly storage: Nova Ponte HEP

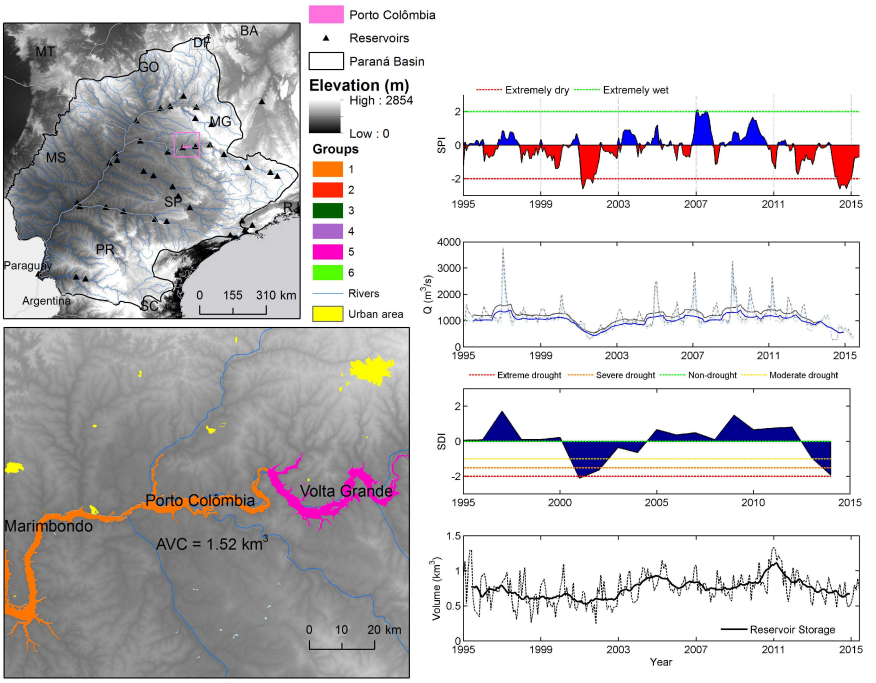

Figure S29. Time series of SDI, SPI and monthly storage: Porto Colômbia HEP

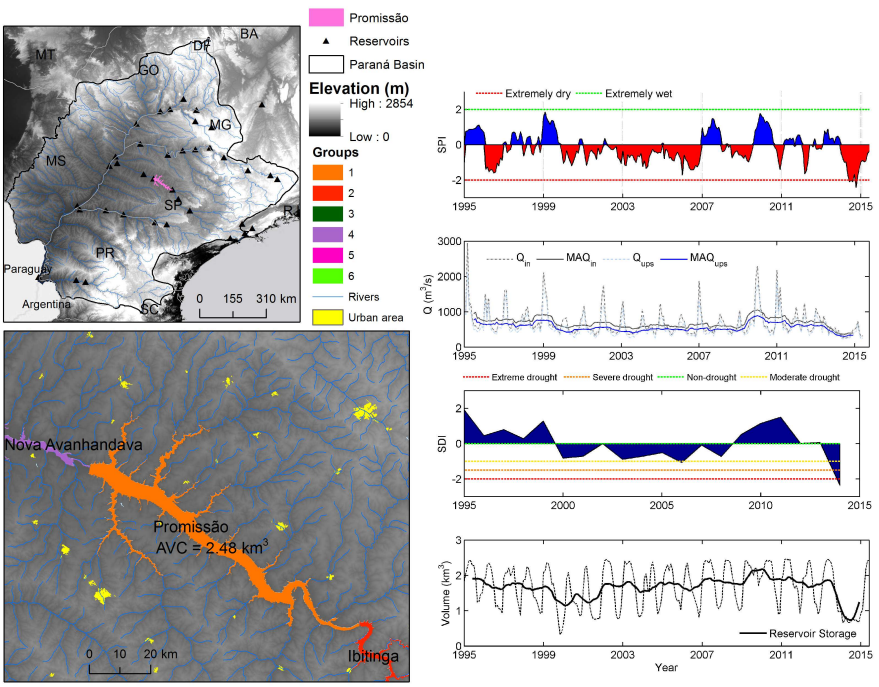

Figure S30. Time series of SDI, SPI and monthly storage: Promissão HEP

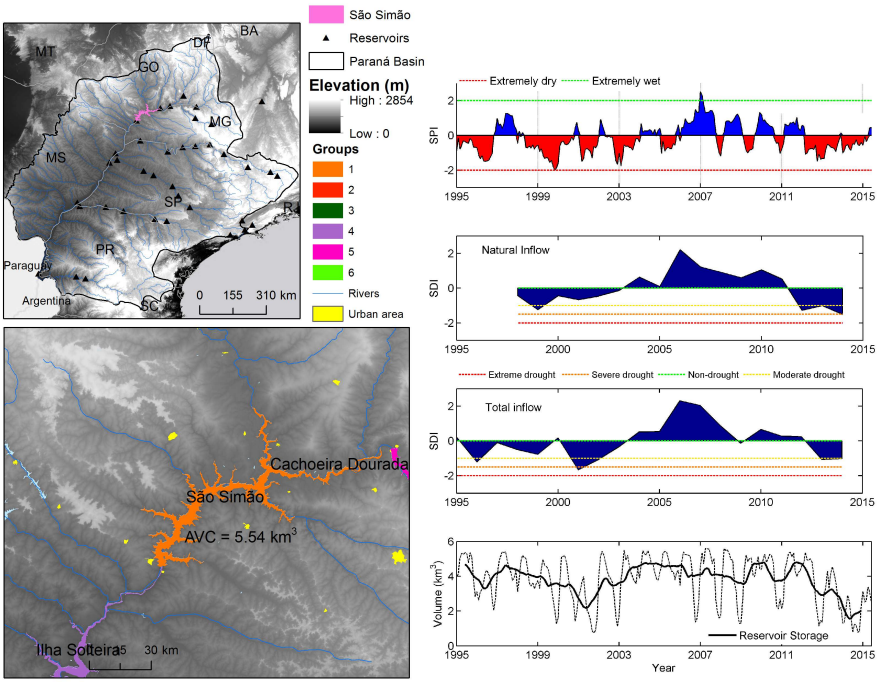

Figure S31. Time series of SDI, SPI and monthly storage: São Simão HEP

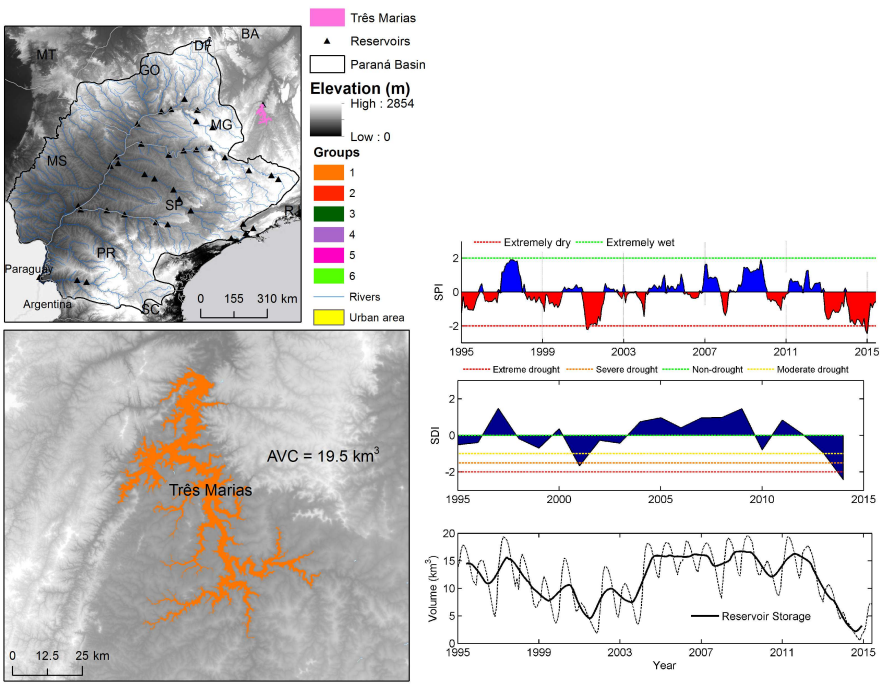

Figure S32. Time series of SDI, SPI and monthly storage: Três Marias HEP

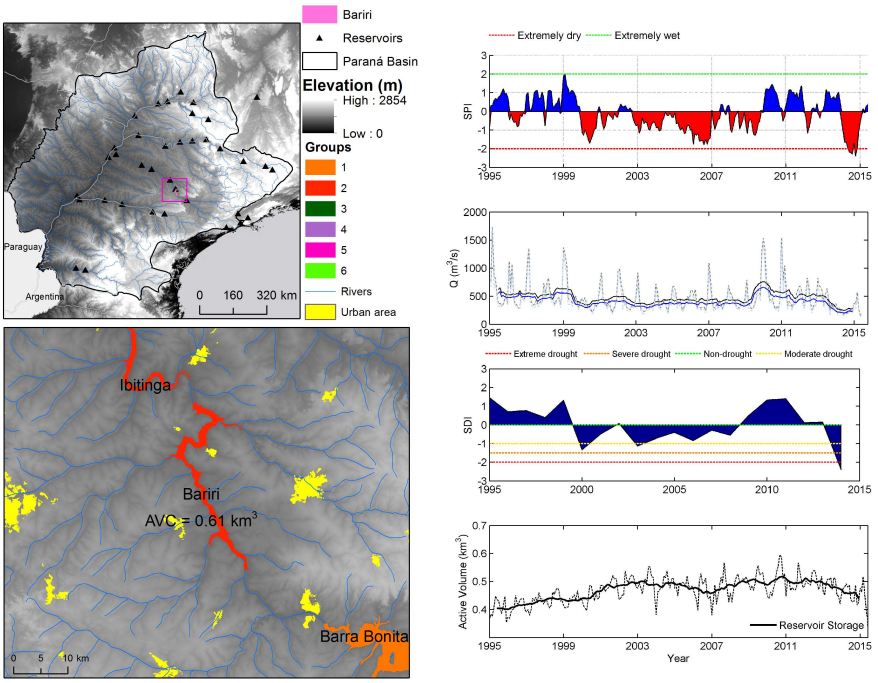

Figure S33. Time series of SDI, SPI and monthly storage: Bariri HEP

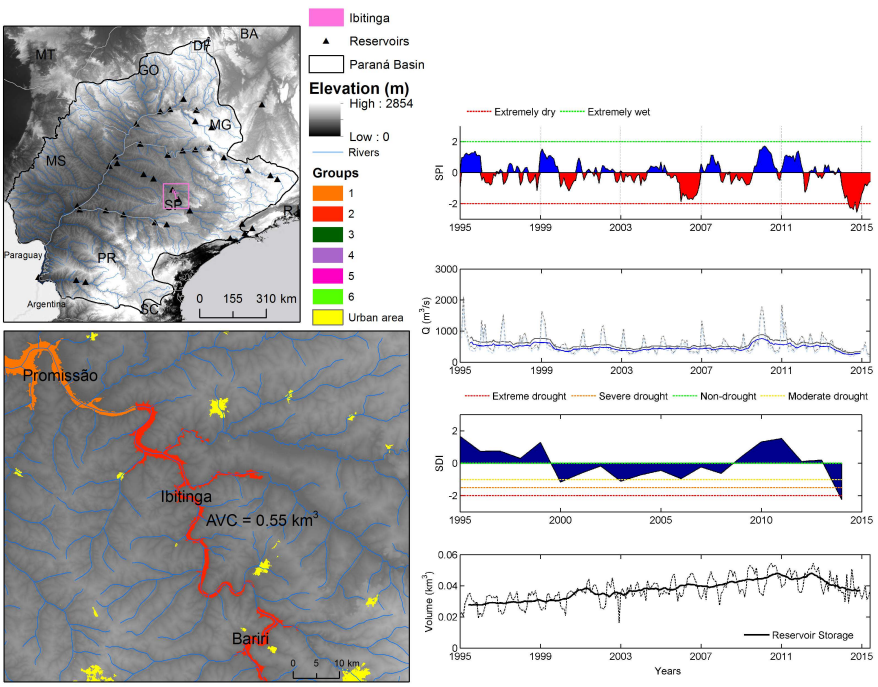

Figure S34. Time series of SDI, SPI and monthly storage: Ibitinga HEP

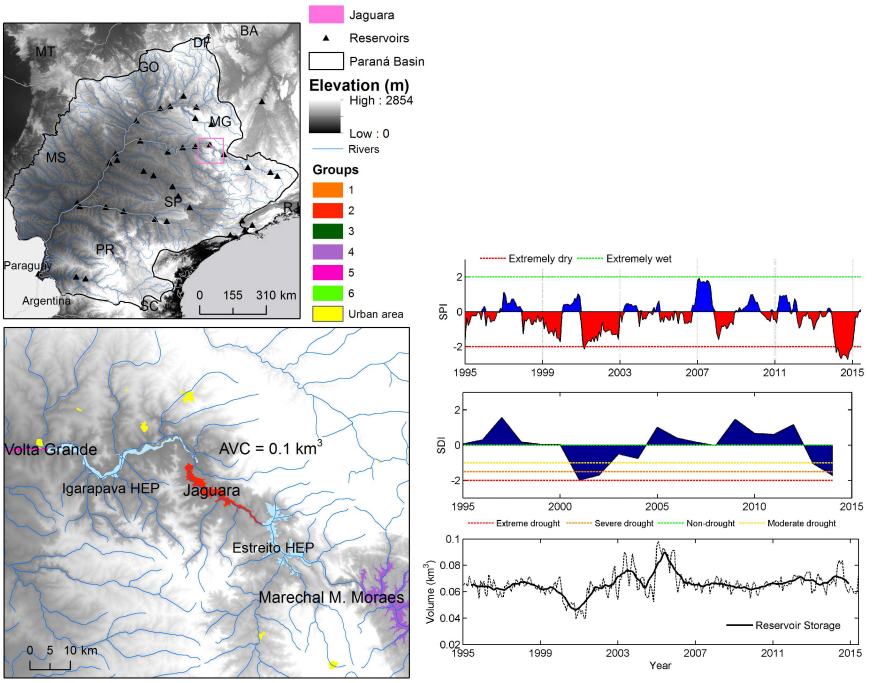

Figure S35. Time series of SDI, SPI and monthly storage: Jaguará HEP

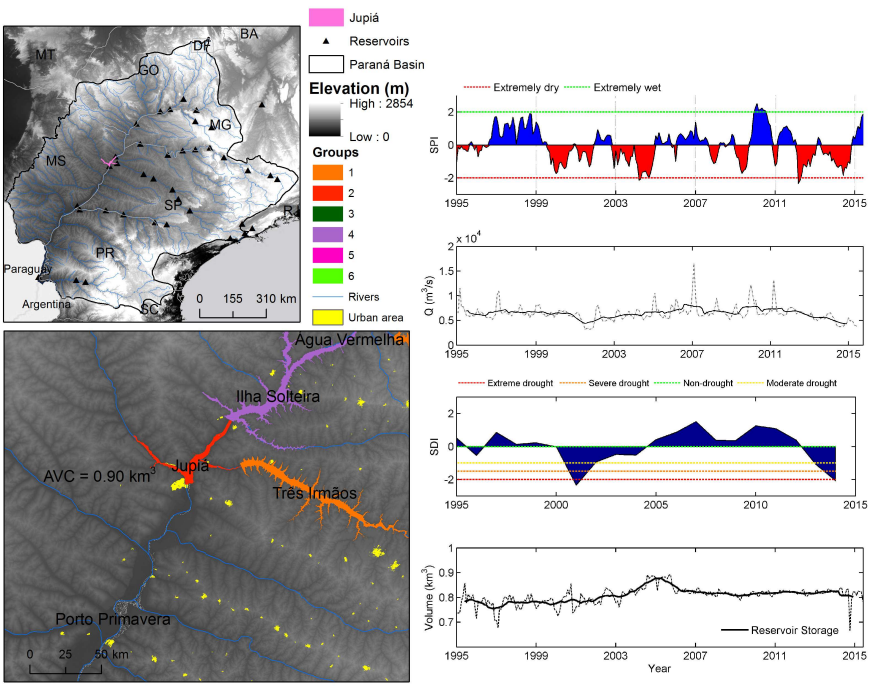

Figure S36. Time series of SDI, SPI and monthly storage: Jupiá HEP

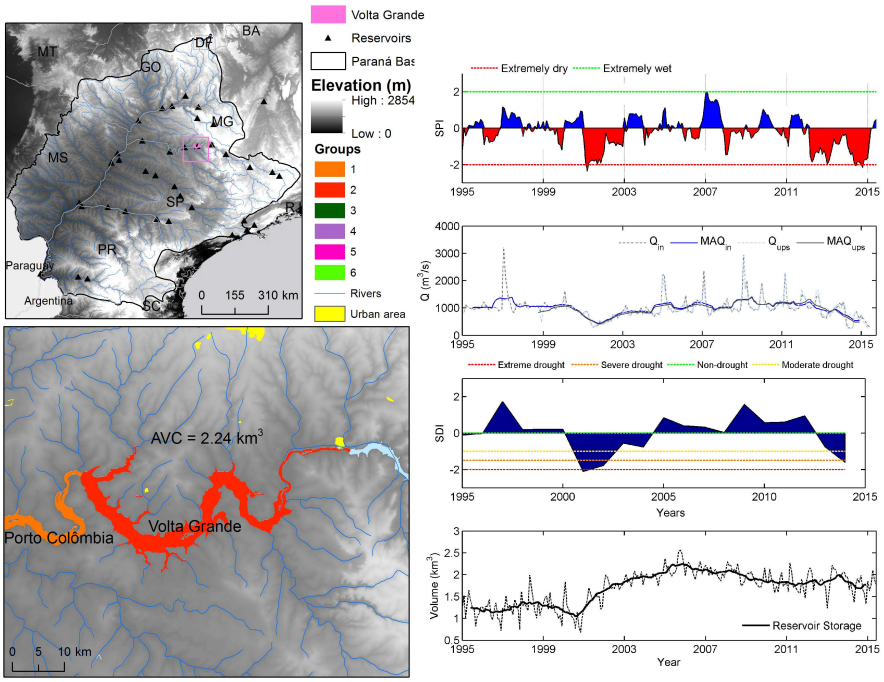

Figure S37. Time series of SDI, SPI and monthly storage: Volta Grande HEP

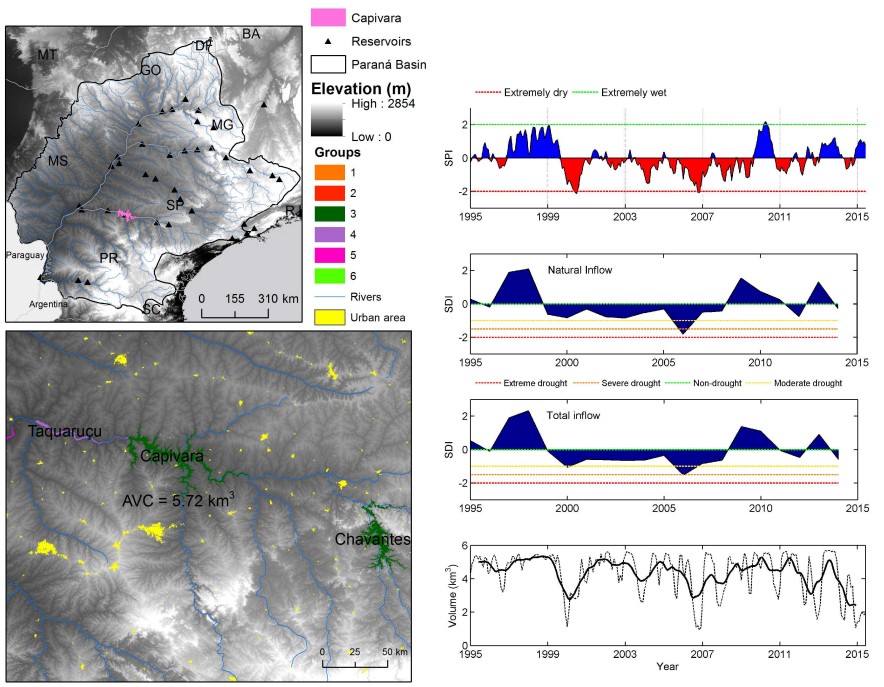

Figure S38. Time series of SDI, SPI and monthly storage: Capivara HEP

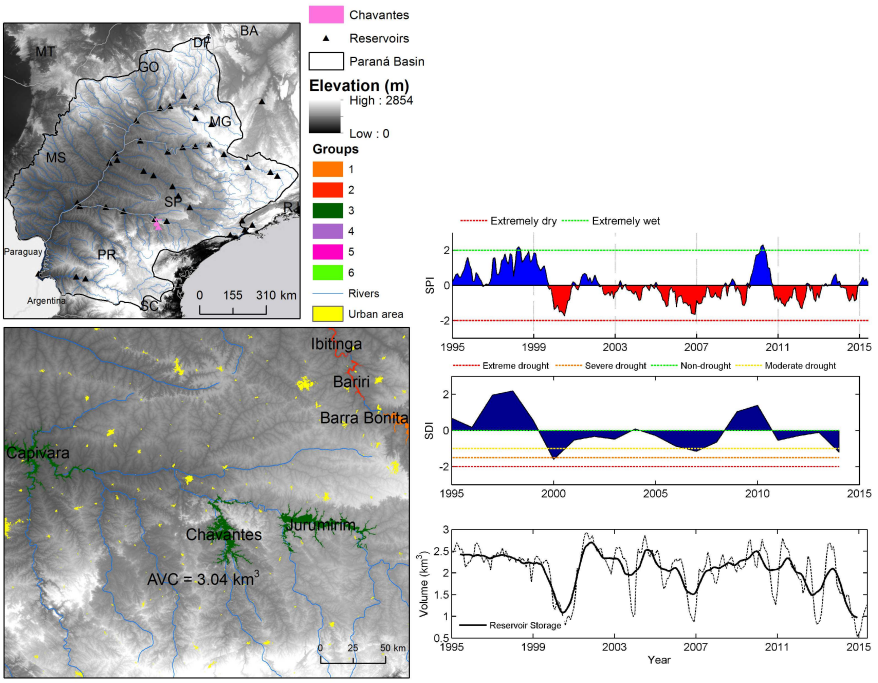

Figure S39. Time series of SDI, SPI and monthly storage: Chavantes HEP

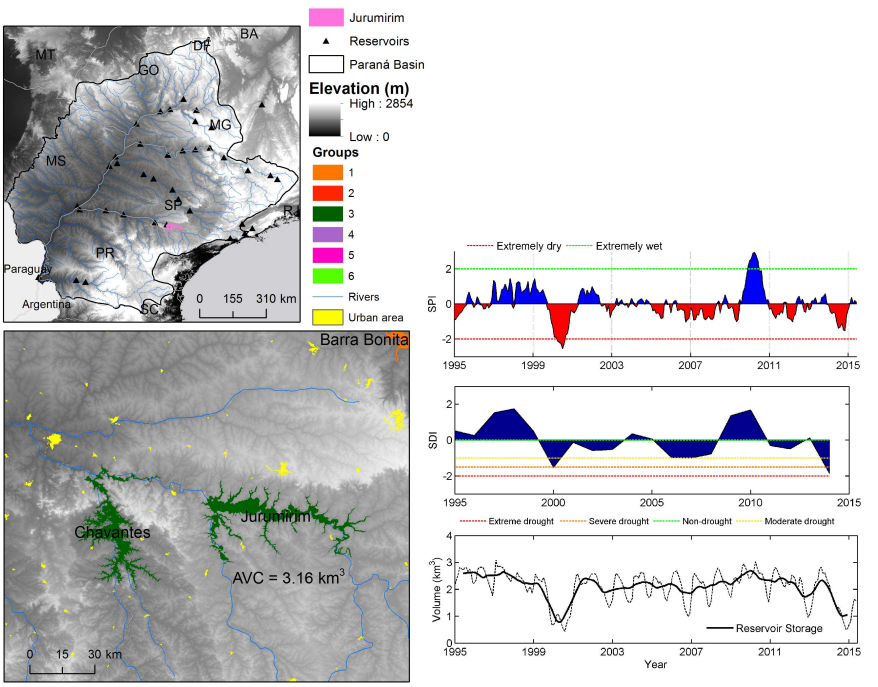

Figure S40. Time series of SDI, SPI and monthly storage: Jurumirim HEP

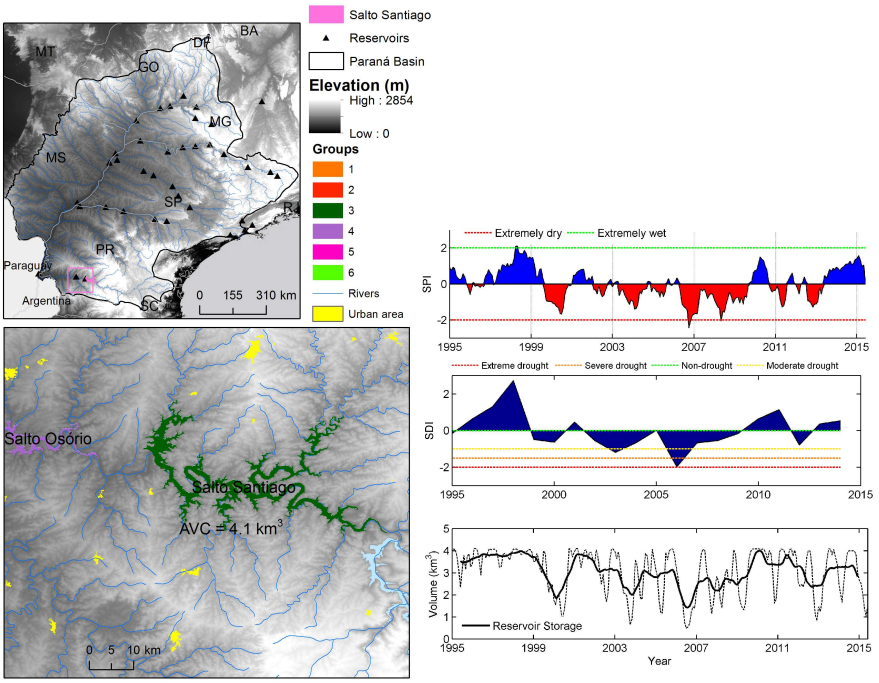

Figure S41. Time series of SDI, SPI and monthly storage: Salto Santiago HEP

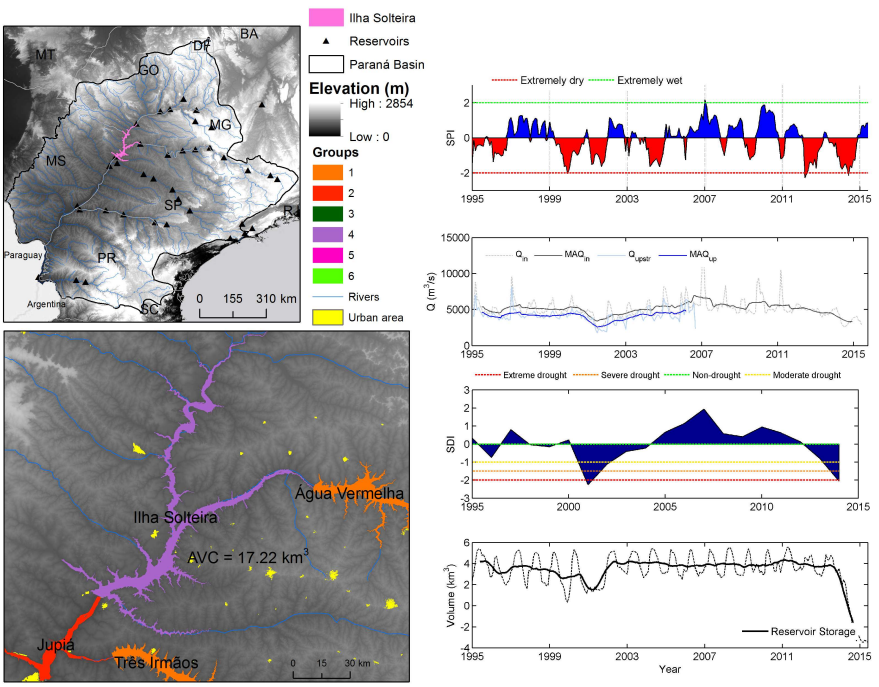

Figure S42. Time series of SDI, SPI and monthly storage: Ilha Solteira HEP

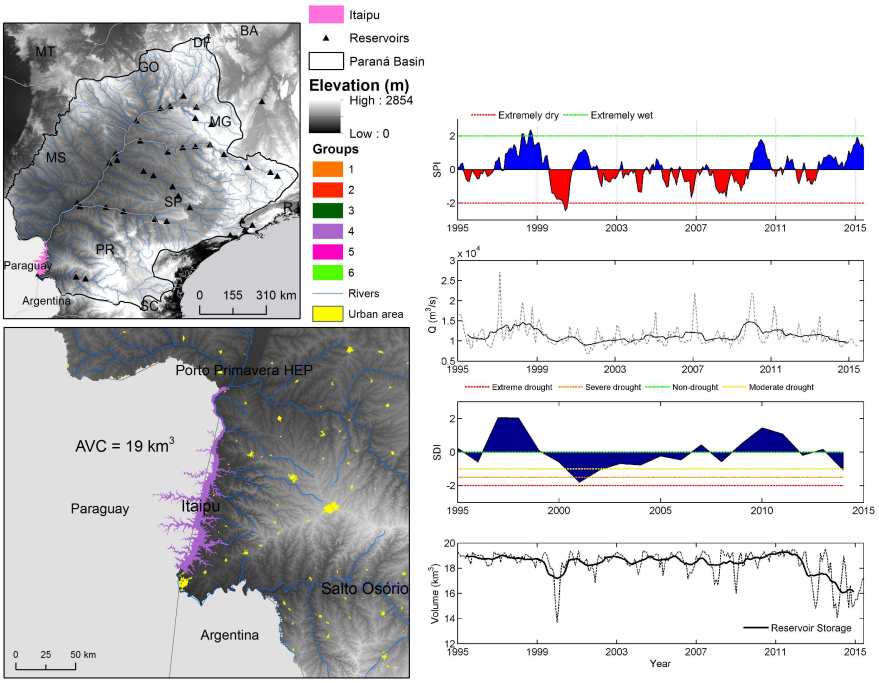

Figure S43. Time series of SDI, SPI and monthly storage: Itaipu HEP

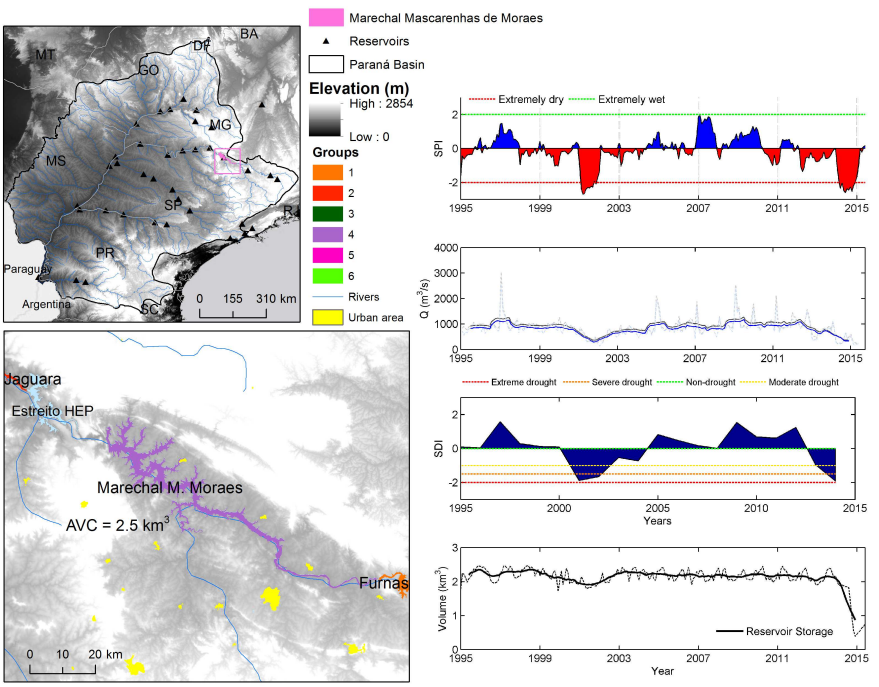

Figure S44. Time series of SDI, SPI and monthly storage: M. M. Moraes HEP

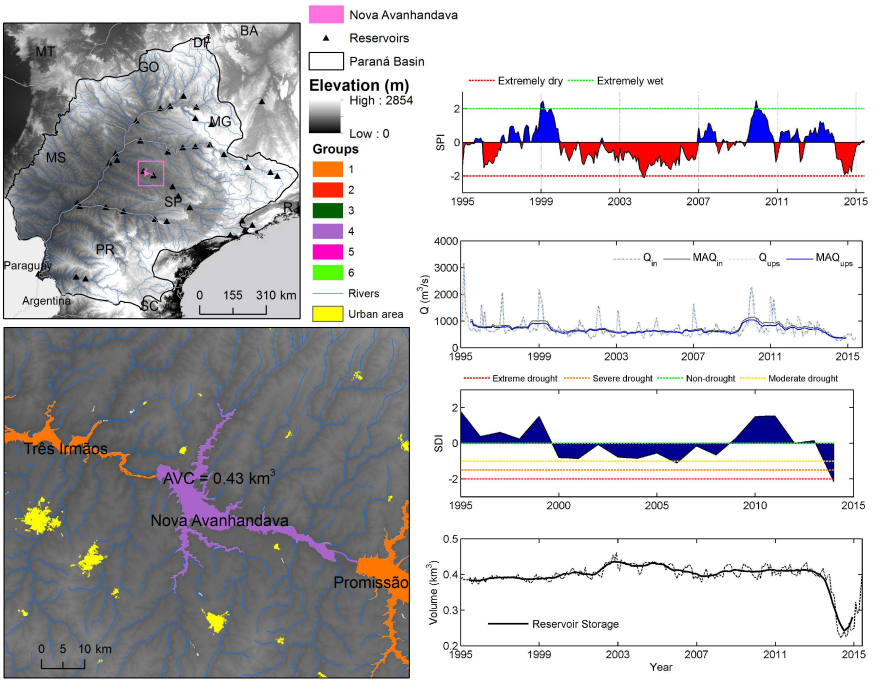

Figure S45. Time series of SDI, SPI and monthly storage: Nova Avanhandava HEP

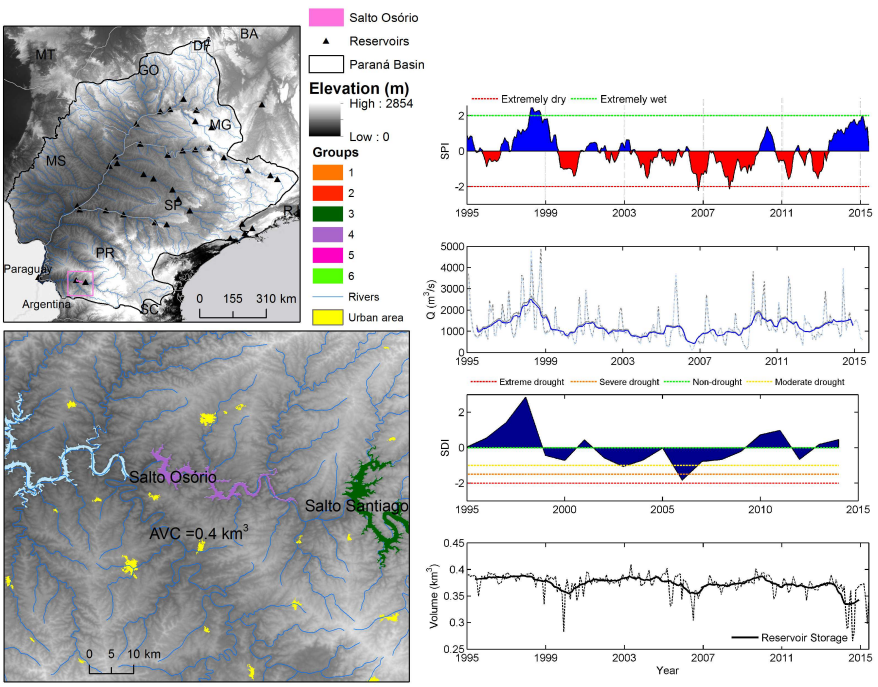

Figure S46. Time series of SDI, SPI and monthly storage: Salto Osório HEP

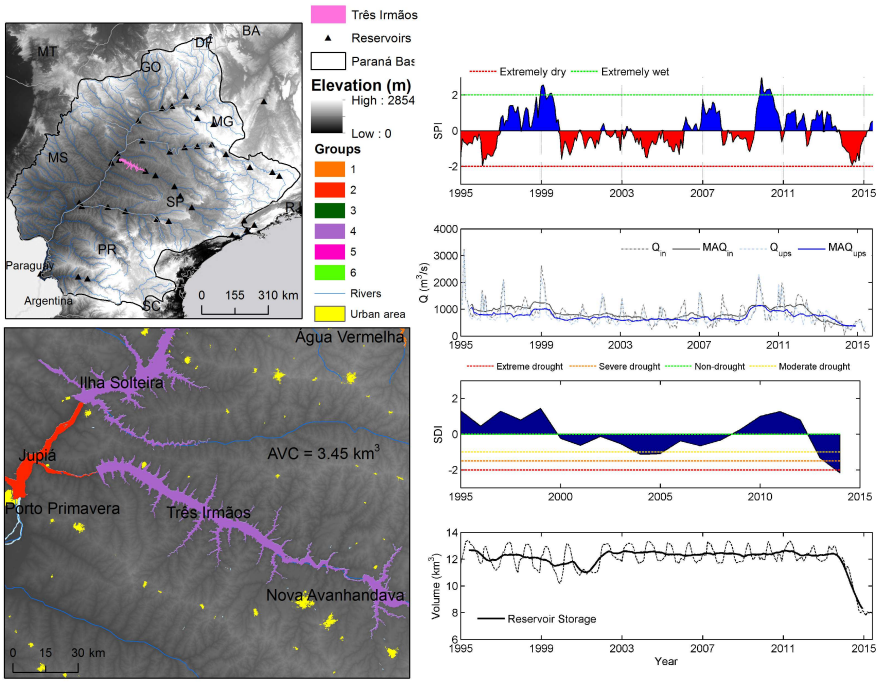

Figure S47. Time series of SDI, SPI and monthly storage: Três Irmãos HEP

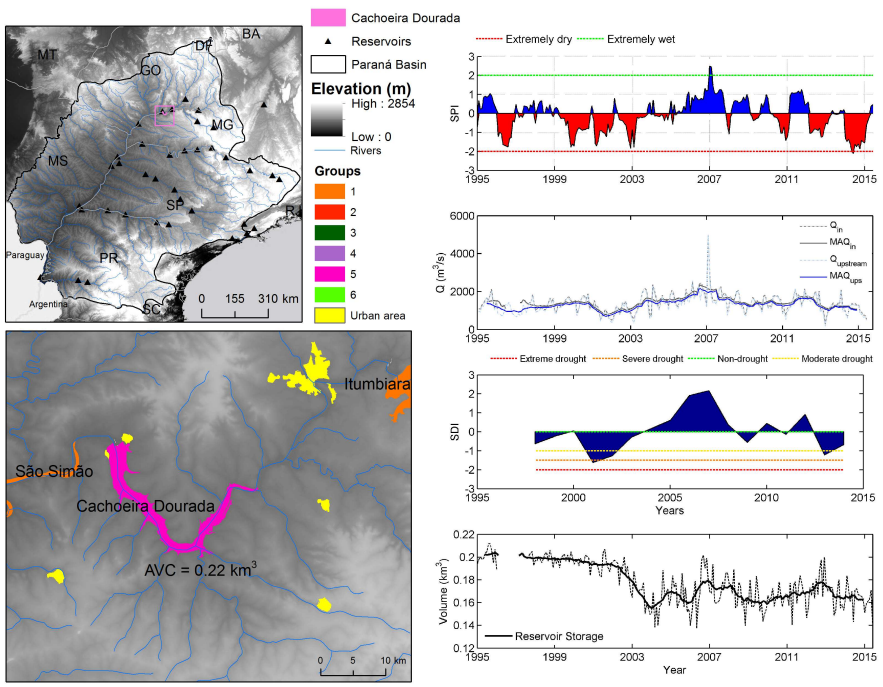

Figure S48. Time series of SDI, SPI and monthly storage: Cachoeira Dourada HEP

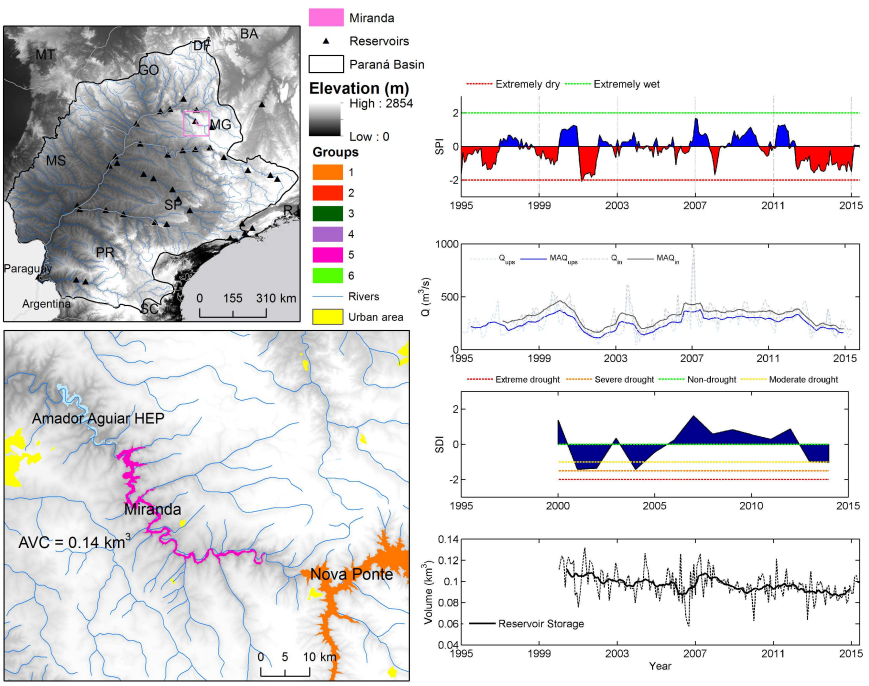

Figure S49. Time series of SDI, SPI and monthly storage: Miranda HEP

All the data used to generate the figures and tables are available as a compressed file in the following link: http://albatroz.shs.eesc.usp.br/?q=dados-de-pesquisa

References

A, G., Wahr, J., and Zhong, S.: Computations of the viscoelastic response of a 3-D compressible Earth to surface loading: an application to Glacial Isostatic Adjustment in Antarctica and Canada, Geophysical Journal International, doi:10.1093/gji/ggs030, http://gji.oxfordjournals.org/content/early/2012/11/16/gji.ggs030.abstract, 2012.

ANA: Caderno da Região Hidrográfica do Paraná, Tech. rep., Ministério do Meio Ambiente, Secretaria de Recursos Hídricos, Brasília, 2006.

ANA: Atlas Brasil: abastecimento urbano de água: panorama nacional, Tech. rep., Agencia Nacional de Aguas, Brasilia, 2010.

Bailey, K. D.: Tipologies and taxonomies: an introduction to classification techniques, Sage University Paper series on Quantitative Applications in the Social Sciences, Thousand Oaks, CA, 1994.

Brito Neto, R. T., Santos, C. A. G., Mulligan, K., and Barbato, L.: Spatial and temporal water-level variations in the Texas portion of the Ogallala Aquifer, Natural Hazards, 80, 351–365, doi:10.1007/s11069-015-1971-8, http://dx.doi.org/10.1007/s11069-015-1971-8, 2015.

Burn, D. H. and Hag Elnur, M. A.: Detection of hydrologic trends and variability, Journal of Hydrology, 255, 107–122, doi:10.1016/S0022-1694(01)00514-5, http://www.sciencedirect.com/science/article/pii/S0022169401005145, 2002.

Chen, F., Mitchell, K., Schaake, J., Xue, Y., Pan, H.-L., Koren, V., Duan, Q. Y., Ek, M., and Betts, A.: Modeling of land surface evaporation by four schemes and comparison with FIFE observations, Journal of Geophysical Research: Atmospheres, 101, 7251–7268, doi:10.1029/95JD02165, http://dx.doi.org/10.1029/95JD02165, 1996.

Cheng, M., Ries, J. C., and Tapley, B. D.: Variations of the Earth's figure axis from satellite laser ranging and GRACE, Journal of Geophysical Research: Solid Earth, 116, n/a–n/a, doi:10.1029/2010JB000850, http://dx.doi.org/10.1029/2010JB000850, b01409, 2011.

Chou, C.-m.: A Threshold Based Wavelet Denoising Method for Hydrological Data Modelling, Water Resources Management, 25, 1809–1830, doi:10.1007/s11269-011-9776-3, http://link.springer.com/article/10.1007/s11269-011-9776-3, 2011.

Coelho, C. A. S., Cardoso, D. H. F., and Firpo, M. A. F.: Precipitation diagnostics of an exceptionally dry event in São Paulo, Brazil, Theoretical and Applied Climatology, pp. 1–16, doi:10.1007/s00704-015-1540-9, http://link.springer.com/article/10.1007/s00704-015-1540-9, 2015a.

Coelho, C. A. S., Oliveira, C. P. d., Ambrizzi, T., Reboita, M. S., Carpenedo, C. B., Campos, J. L. P. S., Tomaziello, A. C. N., Pampuch, L. A., Custódio, M. d. S., Dutra, L. M. M., Rocha, R. P. D., and Rehbein, A.: The 2014 southeast Brazil austral summer drought: regional scale mechanisms and teleconnections, Climate Dynamics, pp. 1–16, doi:10.1007/s00382-015-2800-1, http://link.springer.com/article/10.1007/s00382-015-2800-1, 2015b.

Coutinho, R. M., Kraenkel, R. A., and Prado, P. I.: Catastrophic Regime Shift in Water Reservoirs and São Paulo Water Supply Crisis, PLoS ONE, 10, e0138 278, doi:10.1371/journal.pone.0138278, http://dx.doi.org/10.1371/journal.pone.0138278, 2015.

Cox, D. R. and Stuart, A.: Some Quick Sign Tests for Trend in Location and Dispersion, Biometrika, 42, 80–95, doi:10.2307/2333424, http://www.jstor.org/stable/2333424, 1955.

Dai, Y., Zeng, X., Dickinson, R. E., Baker, I., Bonan, G. B., Bosilovich, M. G., Denning, A. S., Dirmeyer, P. A., Houser, P. R., Niu, G., Oleson, K. W., Schlosser, C. A., and Yang, Z.-L.: The Common Land Model, Bulletin of the American Meteorological Society, 84, 1013–1023, doi:10.1175/BAMS-84-8-1013, http://dx.doi.org/10.1175/BAMS-84-8-1013, 2003.

de Artigas, M. Z., Elias, A. G., and de Campra, P. F.: Discrete wavelet analysis to assess long-term trends in geomagnetic activity, Physics and Chemistry of the Earth, Parts A/B/C, 31, 77–80, doi:10.1016/j.pce.2005.03.009, http://www.sciencedirect.com/science/article/pii/S147470650600012X, 2006.

Derber, J. C., Parrish, D. F., and Lord, S. J.: The New Global Operational Analysis System at the National Meteorological Center, Weather and Forecasting, 6, 538–547, doi:10.1175/1520-0434(1991)006<0538:TNGOAS>2.0.CO;2, http://dx.doi.org/10.1175/1520-0434(1991)006<0538:TNGOAS>2.0.CO;2, 1991.

Ek, M. B., Mitchell, K. E., Lin, Y., Rogers, E., Grunmann, P., Koren, V., Gayno, G., and Tarpley, J. D.: Implementation of Noah land surface model advances in the National Centers for Environmental Prediction operational mesoscale Eta model, Journal of Geophysical Research, 108, 8851, 2003.

Fiorillo, F. and Guadagno, F. M.: Karst Spring Discharges Analysis in Relation to Drought Periods Using the SPI, Water Resources Management, 24, 1867–1884, doi:10.1007/s11269-009-9528-9, http://link.springer.com/article/10.1007/s11269-009-9528-9, 2009.

Gao, P., Mu, X.-M., Wang, F., and Li, R.: Changes in streamflow and sediment discharge and the response to human activities in the middle reaches of the Yellow River, Hydrol. Earth Syst. Sci., 15, 1–10, doi:10.5194/hess-15-1-2011, http://www.hydrol-earth-syst-sci.net/15/1/2011/, 2011.

Getirana, A. C. V.: Extreme water deficit in Brazil detected from space, Journal of Hydrometeorology, doi:10.1175/JHM-D-15-0096.1, http://journals.ametsoc.org/doi/abs/10.1175/JHM-D-15-0096.1, 2015.

Gong, X. and Richman, M. B.: On the Application of Cluster Analysis to Growing Season Precipitation Data in North America East of the Rockies, Journal of Climate, 8, 897–931, doi:10.1175/1520-0442(1995)008<0897:OTAOCA>2.0.CO;2, http://journals.ametsoc.org/doi/abs/10.1175/1520-0442(1995)008%3C0897%3AOTAOCA%3E2.0.CO%3B2, 1995.

Guttman, N. B.: Comparing the Palmer Drought Index and the Standardized Precipitation Index, JAWRA Journal of the American Water Resources Association, 34, 113–121, doi:10.1111/j.1752-1688.1998.tb05964.x, http://onlinelibrary.wiley.com/doi/10.1111/j.1752-1688.1998.tb05964.x/abstract, 1998.

Hamed, K. H.: Trend detection in hydrologic data: The Mann–Kendall trend test under the scaling hypothesis, Journal of Hydrology, 349, 350–363, doi:10.1016/j.jhydrol.2007.11.009, http://www.sciencedirect.com/science/article/pii/S0022169407006865, 2008.

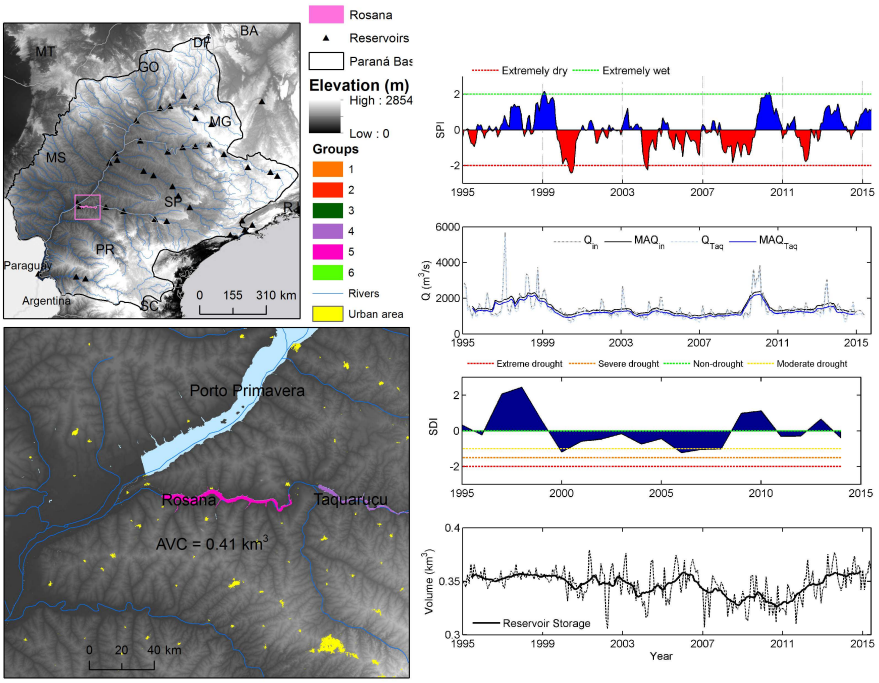

Figure S50. Time series of SDI, SPI and monthly storage: Rosana HEP

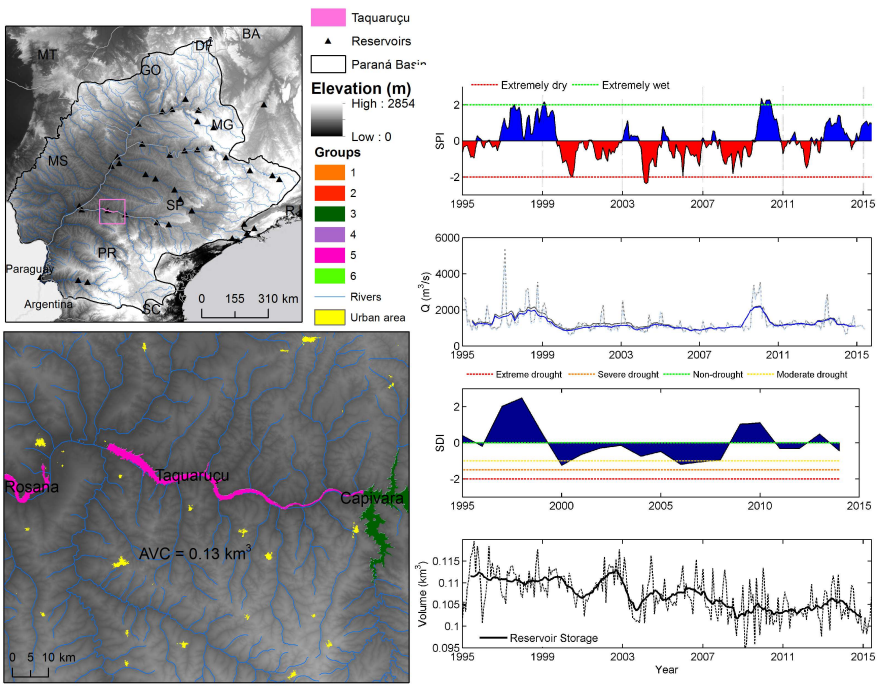

Figure S51. Time series of SDI, SPI and monthly storage: Taquaraçu HEP

Helmer, M. and Hilhorst, D.: Natural disasters and climate change, Disasters, 30, 1–4, doi:10.1111/j.1467-9523.2006.00302.x, http://dx.doi.org/10.1111/j.1467-9523.2006.00302.x, 2006.

Hirsch, R. M. and Slack, J. R.: A non parametric trend test for seasonal data with serial correlation, Water Resources Research, 20, 727–732, 1984.

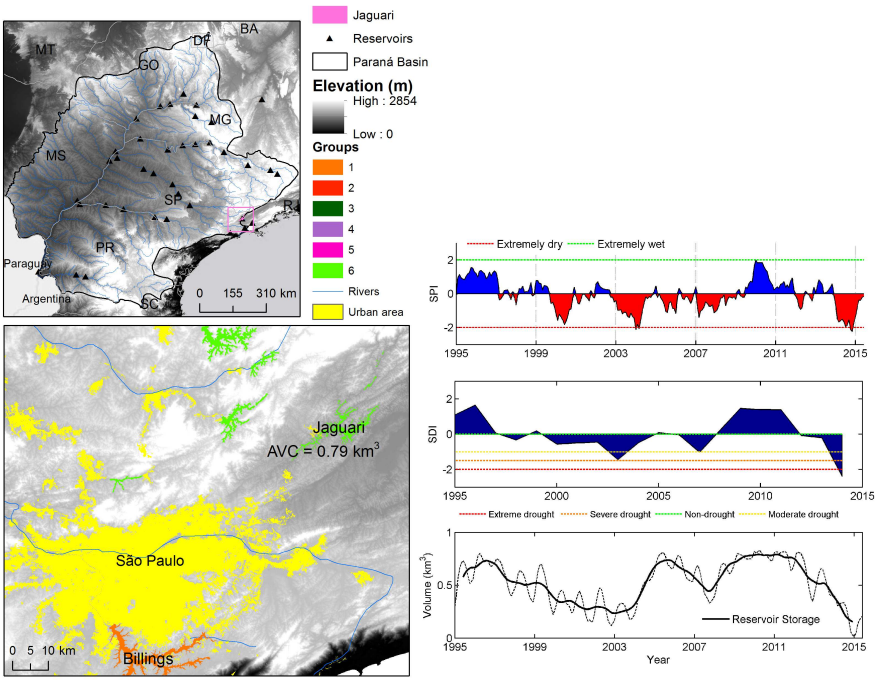

Figure S52. Time series of SDI, SPI and monthly storage: Jaguari HEP

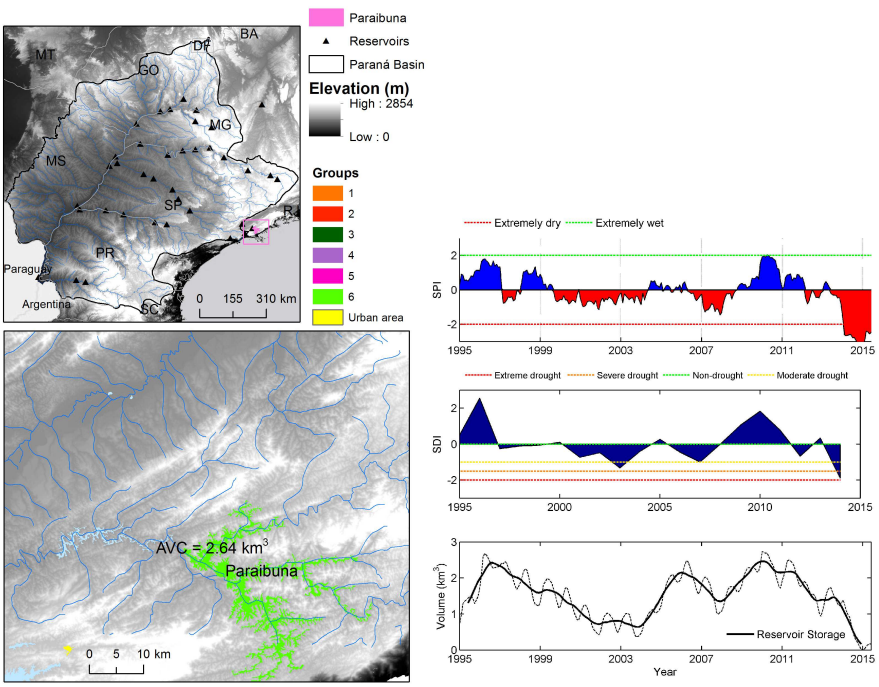

Figure S53. Time series of SDI, SPI and monthly storage: Paraibuna HEP

Huffman, G. J., Adler, R. F., Bolvin, D. T., Gu, G., Nelkin, E. J., Bowman, K. P., Hong, Y., Stocker, E. F., David, and Wolff, B.: The TRMM Multi-satellite Precipitation Analysis: Quasi-Global, Multi-Year, Combined-Sensor Precipitation Estimates at Fine Scale, J. Hydrometeor, pp. 38–55, 2007.

Koster, R. and Suarez, M.: Energy and water balance calculations in the Mosaic LSM, Tech. Memo 9, NASA, 1996.

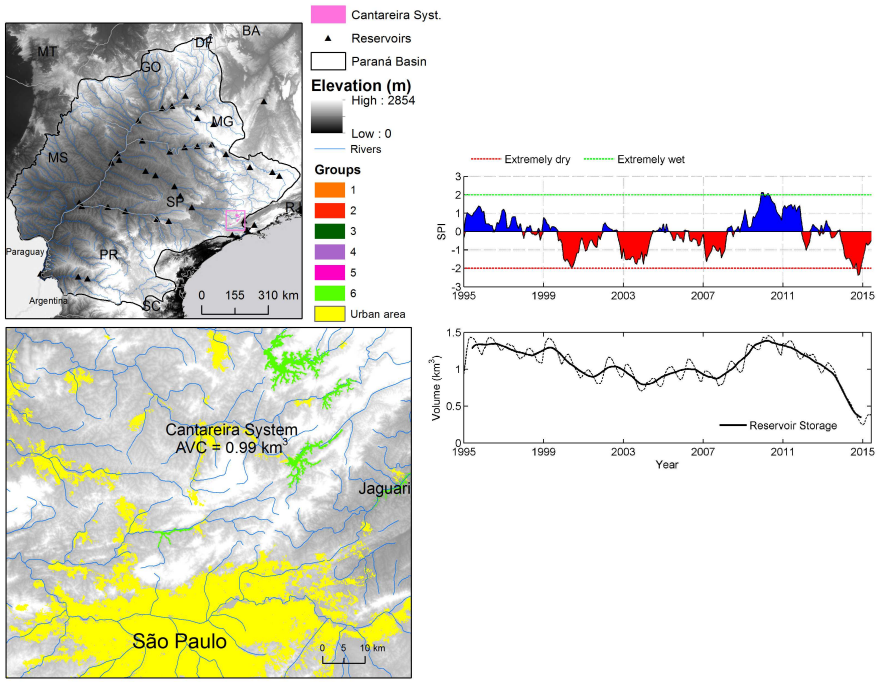

Figure S54. Time series of SDI, SPI and monthly storage: Cantareira System

Liang, X., Lettenmaier, D. P., Wood, E. F., and Burges, S. J.: A simple hydrologically based model of land surface water and energy fluxes for general circulation models, Journal of Geophysical Research: Atmospheres, 99, 14 415–14 428, doi:10.1029/94JD00483, http://dx.doi.org/10.1029/94JD00483, 1994.

Lima, C. H. and Lall, U.: Climate informed monthly streamflow forecasts for the Brazilian hydropower network using a periodic ridge regression model, Journal of Hydrology, 380, 438 – 449, doi:http://dx.doi.org/10.1016/j.jhydrol.2009.11.016, http://www.sciencedirect.com/science/article/pii/S0022169409007252, 2010.

Loarie, S. R., Lobell, D. B., Asner, G. P., Mu, Q., and Field, C. B.: Direct impacts on local climate of sugar-cane expansion in Brazil, Nature Climate Change, 1, 105–109, doi:10.1038/nclimate1067, http://www.nature.com/nclimate/journal/v1/n2/full/nclimate1067.html, 2011.

Mann, H. B. and Whitney, D. R.: On a Test of Whether one of Two Random Variables is Stochastically Larger than the Other, The Annals of Mathematical Statistics, 18, 50–60, http://www.jstor.org/stable/2236101, 1947.

McKee, T. B., Doesken, N. J., and Kleist, J.: Drought Monitoring with Multiple Time Scales, in: 9th AMS Conference on Applied Climatology, pp. 233–236, 1993.

Melo, D. d. C. D., Xavier, A. C., Bianchi, T., Oliveira, P. T. S., Scanlon, B. R., Lucas, M. C., and Wendland, E.: Performance evaluation of rainfall estimates by TRMM Multi-satellite Precipitation Analysis 3B42V6 and V7 over Brazil, Journal of Geophysical Research: Atmospheres, 120, 2015JD023 797, doi:10.1002/2015JD023797, http://onlinelibrary.wiley.com/doi/10.1002/2015JD023797/abstract, 2015.

Mu, Q., Heinsch, F. A., Zhao, M., and Running, S. W.: Development of a global evapotranspiration algorithm based on {MODIS} and global meteorology data, Remote Sensing of Environment, 111, 519 – 536, doi:http://dx.doi.org/10.1016/j.rse.2007.04.015, http://www.sciencedirect.com/science/article/pii/S0034425707001903, 2007.

Mu, Q., Zhao, M., and Running, S. W.: Improvements to a MODIS global terrestrial evapotranspiration algorithm, Remote Sensing of Environment, 115, 1781–1800, doi:10.1016/j.rse.2011.02.019, http://www.sciencedirect.com/science/article/pii/S0034425711000691, 2011.

Nalbantis, I. and Tsakiris, G.: Assessment of Hydrological Drought Revisited, Water Resources Management, 23, 881–897, doi:10.1007/s11269-008-9305-1, http://link.springer.com/article/10.1007/s11269-008-9305-1, 2008.

Nalley, D., Adamowski, J., and Khalil, B.: Using discrete wavelet transforms to analyze trends in streamflow and precipitation in Quebec and Ontario (1954–2008), Journal of Hydrology, 475, 204–228, doi:10.1016/j.jhydrol.2012.09.049, http://www.sciencedirect.com/science/article/pii/S0022169412008669, 2012.

NASA: Tropical Rainfall Measuring Mission, TRMM, senior review proposal, Tech. rep., National Aeronautics and Space Administration, http://pmm.nasa.gov/sites/default/files/document_files/TRMMSenRevProp_v1.2.pdf, 2011.

Popivanov, I. and Miller, R.: Similarity search over time-series data using wavelets, in: 18th International Conference on Data Engineering, 2002. Proceedings, pp. 212–221, doi:10.1109/ICDE.2002.994711, 2002.

Ramana, R. V., Krishna, B., Kumar, S. R., and Pandey, N. G.: Monthly Rainfall Prediction Using Wavelet Neural Network Analysis, Water Resources Management, 27, 3697–3711, doi:10.1007/s11269-013-0374-4, http://link.springer.com/article/10.1007/s11269-013-0374-4, 2013.

Ramoni, M. F., Sebastiani, P., and Kohane, I. S.: Cluster analysis of gene expression dynamics, Proceedings of the National Academy of Sciences, 99, 9121–9126, doi:10.1073/pnas.132656399, http://www.pnas.org/content/99/14/9121, 2002.

Rodell, M., Houser, P. R., Jambor, U., Gottschalck, J., Mitchell, K., Meng, C.-J., Arsenault, K., Cosgrove, B., Radakovich, J., Bosilovich, M., Entin*, J. K., Walker, J. P., Lohmann, D., and Toll, D.: The Global Land Data Assimilation System, Bulletin of the American Meteorological Society, 85, 381–394, doi:10.1175/BAMS-85-3-381, http://journals.ametsoc.org/doi/abs/10.1175/BAMS-85-3-381, 2004.

Rudorff, B. F. T., Aguiar, D. A., Silva, W. F., Sugawara, L. M., Adami, M., and Moreira, M. A.: Studies on the rapid expansion of sugarcane for ethanol production in São Paulo State (Brazil) using Landsat data, Remote Sensing, 2, 1057–1076, 2010.

Ruhoff, A. L., Paz, A. R., Aragao, L. E. O. C., Mu, Q., Malhi, Y., Collischonn, W., Rocha, H. R., and Running, S. W.: Assessment of the MODIS global evapotranspiration algorithm using eddy covariance measurements and hydrological modelling in the Rio Grande basin, Hydrological Sciences Journal, 58, 1658–1676, doi:10.1080/02626667.2013.837578, http://dx.doi.org/10.1080/02626667.2013.837578, 2013.

Sang, Y.-F., Wang, Z., and Liu, C.: Comparison of the MK test and EMD method for trend identification in hydrological time series, Journal of Hydrology, 510, 293–298, doi:10.1016/j.jhydrol.2013.12.039, http://www.sciencedirect.com/science/article/pii/S0022169413009360, 2014.

Storch, H.: Analysis of Climate Variability: Applications of Statistical Techniques Proceedings of an Autumn School Organized by the Commission of the European Community on Elba from October 30 to November 6, 1993, chap. Misuses of Statistical Analysis in Climate Research, pp. 11–26, Springer Berlin Heidelberg, Berlin, Heidelberg, doi:10.1007/978-3-662-03744-7_2, http://dx.doi.org/10.1007/978-3-662-03744-7_2, 1999.

Swenson, S. and Wahr, J.: Post-processing removal of correlated errors in GRACE data, Geophysical Research Letters, 33, n/a–n/a, doi:10.1029/2005GL025285, http://dx.doi.org/10.1029/2005GL025285, l08402, 2006.

Teodoro, P. E., Correa, C. C. G., Torres, F. E., de Oliveira-Junior, J. F., da Silva Junior, C. A., Gois, G., and Delgado, R. C.: Analysis of the Occurrence of Wet and Drought Periods Using Standardized Precipitation Index in Mato Grosso do Sul State, Brazil, Journal of Agronomy, 14, 80–86, doi:10.3923/ja.2015.80.86, 2015.

Vicente-Serrano, S. M. and López-Moreno, J. I.: Hydrological response to different time scales of climatological drought: an evaluation of the Standardized Precipitation Index in a mountainous Mediterranean basin, Hydrol. Earth Syst. Sci., 9, 523–533, doi:10.5194/hess-9-523-2005, http://www.hydrol-earth-syst-sci.net/9/523/2005/, 2005.

Vonesch, C., Blu, T., and Unser, M.: Generalized Daubechies Wavelet Families, IEEE Transactions on Signal Processing, 55, 4415–4429, doi:10.1109/TSP.2007.896255, 2007.

Ward, J. H.: Hierarchical Grouping to Optimize an Objective Function, Journal of the American Statistical Association, 58, 236–244, doi:10.1080/01621459.1963.10500845, http://www.tandfonline.com/doi/abs/10.1080/01621459.1963.10500845, 1963.

Wei, S., Song, J., and Khan, N. I.: Simulating and predicting river discharge time series using a wavelet-neural network hybrid modelling approach, Hydrological Processes, 26, 281–296, doi:10.1002/hyp.8227, http://onlinelibrary.wiley.com/doi/10.1002/hyp.8227/abstract, 2012.

Xavier, A. C., King, C. W., and Scanlon, B. R.: Daily gridded meteorological variables in Brazil (1980–2013), International Journal of Climatology, pp. n/a–n/a, doi:10.1002/joc.4518, http://dx.doi.org/10.1002/joc.4518, 2015.

Zhang, K., Kimball, J. S., Nemani, R. R., and Running, S. W.: A continuous satellite-derived global record of land surface evapotranspiration from 1983 to 2006, Water Resources Research, 46, W09 522, doi:10.1029/2009WR008800, http://onlinelibrary.wiley.com/doi/10.1029/2009WR008800/abstract, 2010.

Zhang, X., Harvey, K. D., Hogg, W. D., and Yuzyk, T. R.: Trends in Canadian streamflow, Water Resources Research, 37, 987–998, doi:10.1029/2000WR900357, http://onlinelibrary.wiley.com/doi/10.1029/2000WR900357/abstract, 2001.

Zhang, Z., Chao, B., Chen, J., and Wilson, C.: Terrestrial water storage anomalies of Yangtze River Basin droughts observed by GRACE and connections with ENSO, Global and Planetary Change, 126, 35 – 45, doi:http://dx.doi.org/10.1016/j.gloplacha.2015.01.002, http://www.sciencedirect.com/science/article/pii/S092181811500017X, 2015.

Zhang, Z.-Z., Chao, B. F., Lu, Y., and Hsu, H.-T.: An effective filtering for GRACE time-variable gravity: Fan filter, Geophysical Research Letters, 36, n/a–n/a, doi:10.1029/2009GL039459, http://dx.doi.org/10.1029/2009GL039459, l17311, 2009.